5-2004

Ti-8Mo as an Alternative to Ti-6Al-4V in Hip Replacement Implants

Brandice Annette Green
University of Tennessee, Knoxville

To the Graduate Council:

I am submitting herewith a thesis written by Brandice Annette Green entitled "Ti-8Mo as an Alternative to Ti-6Al-4V in Hip Replacement Implants." I have examined the final electronic copy of this thesis for form and content and recommend that it be accepted in partial fulfillment of the requirements for the degree of Master of Science, with a major in Materials Science and Engineering.

Raymond A. Buchanan, Major Professor

We have read this thesis and recommend its acceptance:

Peter Liaw, Roberto Benson

Accepted for the Council:
Carolyn R. Hodges

Vice Provost and Dean of the Graduate School

(Original signatures are on file with official student records.)

To the Graduate Council:

I am submitting herewith a thesis written by Brandice Annette Green entitled "Ti-8Mo as an Alternative to Ti-6Al-4V in Hip Replacement Implants." I have examined the final paper copy of this thesis for form and content and recommend that it be accepted in partial fulfillment of the requirements for the degree of Master of Science, with a major in Materials Science and Engineering.

R. A. Buchanan

Raymond A. Buchanan, Major Professor

We have read this thesis
and recommend its acceptance:

Peter K. Liaw

Roberto Benson

Accepted for the Council:

Vice Chancellor and Dean of Graduate Studies

TI-8MO AS AN ALTERNATIVE TO TI-6AL-4V IN HIP REPLACEMENT IMPLANTS

A Thesis
Presented for the
Master of Science
Degree
The University of Tennessee, Knoxville

Brandice Annette Green
May 2004

DEDICATION

This thesis is dedicated to my parents, Archie and Barbara Green, who have instilled in me that faith in God and hard work make all goals attainable, to my best friends Brandon Weathers and Victoria Venable, who have taught me not to take myself so seriously, and the rest of my friends and family for their love, encouragement, and support.

ACKNOWLEDMENTS

I would like to first thank Dr. Raymond Buchanan for all of his suggestions and invaluable guidance. Also, thanks to Drs. Roberto Benson and Peter Liaw for all of their direction with my research. Thanks to Dr. Peter Blau in the Surface Processing and Mechanics Group of the Metals and Ceramics Division for allowing me to use the profilometers at Oak Ridge National Laboratories. Thanks to Mark Morrison for help with profilometry, William Peter for assistance with the corrosion software, Irene Paulauskas for help with the wear machine, and Christopher Stephens for help with the MATLAB program. Also thanks to Doug Fielden for machining samples. Thank you to all NSF-IGERT group members especially research effort 2 for all their encouragement. Last but not least, I would like to thank Carla Lawrence and Sandra Maples in the Materials Science and Engineering office for their kindness and assistance.

ABSTRACT

In the present research, the wear and corrosion properties of a heat treated Ti-8Mo alloy are compared to that of Ti-6Al-4V, an alloy commonly used as the material for the stem component of hip prostheses. Ti-6Al-4V has the attractive properties of high strength to weight ratio and excellent corrosion resistance. However, the alloy has poor wear resistance and there have been biocompatibility concerns with Al and V. The heat treated Ti-8Mo is an alloy that has not yet been examined for biomaterial applications. However, the low toxicity of Mo and the possibility of improved wear resistance due to heat treatment warrant the consideration of Ti-8Mo as an alternative to Ti-6Al-4V in hip replacement implants.

Ti-6Al-4V ELI plates were donated by Titanium Industries, Inc. The Ti-6Al-4V plates were machined at The University of Tennessee into flat disks. Ti-8Mo was fabricated by arc melting in an inert argon atmosphere. The material was held at 925°C for 16 hours, immediately transferred to a furnace at 776°C and isothermally aged for 2 hours in the $\alpha + \beta$ region, then water quenched to room temperature. This heat treatment was performed as described by James and Moon [9] to obtain a microstructure of a precipitated ω phase in a $\alpha + \beta$ matrix. James and Moon demonstrated that the ω phase was associated with increases in hardness and strength, which inferred that the ω phase could lead to improved wear resistance. Ti-8Mo was also machined into flat disks at The University of Tennessee.

Pin-on-disk wear tests with PMMA pins were performed on Ti-6Al-4V and Ti-8Mo in a bovine serum (simulation of synovial fluid) at room temperature. The contact stress of the pin was 3.4 MPa with an interfacial velocity of 150 mm/s. During wear tests, a hold potential of 100 mV above the open-circuit-potential was applied, and the current was measured. Profilometry was used to quantify the total material loss for each alloy. Cyclic-anodic-polarization experiments were conducted in a phosphate buffered saline (PBS) solution at 37°C. The oxygen concentration of the solution was controlled by aerating the solution with a N_2 gas mixture containing 0.4 % O_2. The flow rate of the gas mixture was approximately 50 mL/s. Corrosion rate calculations were performed for each alloy to predict the amount of material lost in one year.

The total mass loss of Ti-6Al-4V was more than 10 times that of Ti-8Mo. The average mass loss value due to wear for Ti-6Al-4V was greater than 10 times that of Ti-8Mo. For both alloys, the amount of material loss due to corrosion was significantly lower than that lost due to wear. Cyclic-anodic-polarization results supported that both Ti-6Al-4V and Ti-8Mo were extremely resistant to localized corrosion in the simulated biological environment. And, both alloys exhibited low corrosion current densities and low corrosion penetration rates. Overall, the pin-on-disk wear behavior of Ti-8Mo was superior to that of Ti-6Al-4V, and Ti-8Mo exhibited excellent corrosion resistance that was comparable to that of Ti-6Al-4V.

TABLE OF CONTENTS

LIST OF TABLES

LIST OF FIGURES

CHAPTER 1: BACKGROUND

Metallic materials have been utilized in the body for many years. Before the effects of certain materials in the body were considered, metals such as brass, copper, silver, nickel-plated steel, and high carbon steel were all implemented as implants in surgery [1]. However, experiments began to reveal that some metals had adverse effects on the body. Moderately successful metal alloys were introduced in the late 1920s, but these alloys lacked the adequate corrosion resistance required to withstand the body's environment [1].

The 1940s marked the emergence of titanium as a material for surgical implants in the United States [2]. The excellent tissue compatibility of titanium was first verified by early animal experiments by Bothe et al. [1-4] and Leventhal [2, 5]. The electrochemical work of Clarke and Hickmen confirmed the exceptional corrosion resistance of titanium [1, 4]. Nevertheless in the 1950s and 1960s, only a few titanium internal fixation devices were used in the United States. However, in England, titanium alloy devices were widely used [2].

In the early 1970s, commercially pure titanium began gaining widespread use as an implant material [2]. Although commercially pure titanium offered superior corrosion resistance and tissue tolerance in comparison to stainless steels, it did not have comparable mechanical properties to the implant materials of the day [2]. The hardness, tensile strength, and the yield strength of titanium were considerably less than the stainless steel implants being used at the time [1-2, 4]. These factors and unfavorable tribological properties led to titanium's use being limited to applications in pacemaker cases, heart-valve cages, and reconstruction devices [2].

The discovery that titanium alloys had superior mechanical properties and comparable corrosion resistance facilitated gained interest in experimenting with titanium alloys for surgical implants. Toward the late 1970s, there was a growing interest in the titanium-6aluminum-4vanadium alloys (Ti-6Al-4V) for total joint prostheses due to its high strength-to-weight ratio, low elastic modulus, excellent corrosion resistance, and good tissue tolerance [2].

Today, Ti-6Al-4V is the most prevalent and most studied titanium alloy. The alloy has good strength while preserving its ductility and has a Young's modulus closer to bone than other biomedical alloys. Nevertheless, there are concerns with possible long-term biological effects of the alloying elements and poor tribological properties of the alloy [6-8]. Not only are there possible biological effects associated with Ti-6Al-4V, but the tribological behavior of Ti-6Al-4V has frequently been reported to be poor due to a high coefficient of friction and poor performance under abrasive and adhesive wear. The wear performance of this material is of great concern due to normal activities, such as walking, that can cause friction between implant components.

Much of the current research uses surface modification techniques in attempts to improve the tribological properties of Ti-6Al-4V in order to increase the life of hip-replacement implants. However, this approach does not address the possible biocompatibility problems of Al and V. A titanium alloy with improved tribological behavior, better biocompatibility, and comparable corrosion resistance and modulus could serve as an alternative to Ti-6Al-4V in joint implants.

In this research, a titanium-8molybdenum, Ti-8Mo, was isothermally aged to facilitate the formation of ω precipitates. This heat treatment was chosen based on the research of James and Moon [9] that documented changes of the mechanical properties of three binary alloys (Ti-8Mo, Ti-12V, and Ti-17Nb) due to the various heat treatments. James and Moon detected an abrupt change in mechanical properties when quenching was performed at temperatures in the region of the $\beta/(\alpha+\beta)$ transition. When the quenching temperature was decreased through a temperature range of 10°C, the elastic modulus, hardness, and tensile strength rose significantly. The study reported that Ti-8Mo exhibited a hardness maximum (333 HV) at a quench temperature of 802°C. However, at this temperature, the elastic modulus of Ti-8Mo (104 GPa) was comparable to that of Ti-6Al-4V. Ho et al. [10] observed that an isothermally aged Ti-7.5Mo with a martensitic structure had a bending modulus of 55 GPa, 47% lower than that of Ti-6Al-4V.

The documented high hardness of Ti-8Mo suggests that the alloy may have acceptable wear resistance. The Ti-8Mo alloy also addresses the problem of biocompatibility issues associated with Al and V. Mo is labeled as a non-toxic element [11] and is categorized in the capsule-forming group [11, 12]. Figure 1 [11] illustrates the biological safety of selective metals (all figures located in *Appendix of Figures* section). Messer and Lucas [13] conducted experiments that evaluated viability, lysosomal activity, oxygen consumption, and membrane activity of fibroblasts that had been exposed to salt solutions containing various ions. The study concluded that Mo^{6+} was least toxic. A biocompatibility review by Geursten [14] supports the good biocompatibility of Mo. Table 1 [14] (all tables located in *Appendix of Tables* section) ranks the cytotoxicity of various metal ions evaluated in L-929 or 3T3 mouse fibroblast cultures as reported from various studies. Zardiackas et al. [15] concluded that subcutaneous screening tests and animal implantation suggested that Ti-15Mo had a satisfactory localized biological response when compared to Ti-6Al-4V and Ti-6Al-7Nb.

The promise of good wear resistance combined with a low modulus and good biocompatibility warrants the examination of Ti-8Mo as an alternative to Ti-6Al-4V. Thus, in the current research, the wear resistance of Ti-8Mo was evaluated to determine if it is better or comparable to that of Ti-6Al-4V. The electrochemical behavior of Ti-8Mo is also monitored to determine if the alloy has adequate corrosion resistance to endure in a biological environment.

CHAPTER 2: TOTAL HIP ARTHROPLASTY

Arthroplasty is the repair of a diseased joint to improve its function and reduce the pain [16]. There are various ways to repair a diseased joint, but the most common procedure is by completely replacing the damaged joint. Total joint replacement (TJR) is one of the most commonly performed and successful procedures in modern orthopedic surgery. The high success rates have led to a steady increase in popularity with more than 1 million joint replacement procedures performed annually worldwide [17]. In 2002, hip implants produced revenues of 1.2 billion dollars in the United States alone [18]. The large impact of this industry illustrates why there has been increased interest in research on materials suitable for total joint replacement.

2.1 REASONS FOR TOTAL HIP REPLACEMENT (THR)

Arthritis is defined as inflammation of the joints. Prolonged inflammation can go on to cause permanent damage to the cartilage in the joints and is the main cause of total joint replacement. There are several different types of arthritis, such as rheumatoid arthritis and avascular necrosis. However, osteoarthritis is the most common form of arthritis in the United States and usually occurs in people over 40 [19]. Osteoarthritis, or "wear and tear" is the main cause of total hip-replacement surgery [19-20].

Figure 2 illustrates the two main components of the hip joint: the acetabulum, the rounded socket in the pelvis, and the femoral head, which fits into the socket. The femoral head and socket are held together by ligaments to offer stability. The synovial membrane covers the remaining surfaces of the hip joint. In a healthy hip, this membrane provides fluid that lubricates and decreases friction in the joint. Smooth articular cartilage that enable the bones to move easily cover the surfaces of the acetabulum and the femoral heard. Due to osteoarthritis, the cartilage in the hip joints is worn away. The synovial membrane thickens due to the absorption of the worn cartilage [16, 19-21]. The removal of the cartilage causes the femoral head to experience elevated friction that may cause abnormalities of the bone and misalignment of the joint. These conditions are painful and usually lead to the replacement of the damaged hip joint.

2.2 DISCUSSION OF HIP PROSTHESES

An illustration of a total hip replacement (THR) prosthesis is shown in Figure 3. One of the most prevalent designs of the hip implant consists of a metal femoral prosthesis that is secured in the thigh bone by poly(methyl methacrylate) (PMMA) and a acetabulum component made of ultrahigh-molecular weight linear polyethylene (UHMWPE), also secured with PMMA [22] in the socket of the pelvis. The long bones of the lower body act primarily as load bearing members. For this reason, the femoral component of a hip implant is generally metal. Common metals that have been utilized for the femoral component are stainless steels and Co-Cr-Mo alloys. However, the stiffness of these alloys greatly exceeds the elastic modulus of the bone of the hip joint, cortical bone (17-24 GPa) [22]. This difference in the stiffness between bone and the metal of the femoral component leads to stress shielding, which can cause bone loss and loosening of the

implant [22]. The concerns about stress shielding have lead to the use of Ti-6Al-4V as the material for the femoral component. Ti-6Al-4V has an elastic modulus (105 GPa) that is still higher than that of bone but significantly lower than that of stainless steel and Co-Cr-Mo. Ti-6Al-4V is also used because of its excellent corrosion resistance and lightweight. Ti-6Al-4V has a specific gravity of 4.4 compared with 8.0 and 8.3 for stainless steel and Co-Cr-Mo, respectively [23].

2.3 SIGNIFICANCE OF WEAR IN THR

Wear and the production of wear debris are recognized as the limiting factors in the life of hip prostheses [24-25]. In a healthy functioning hip, the friction of the articular surfaces is greatly decreased due to the lubricating synovial membrane and the smooth cartilage that covers the bones. The coefficient of friction of the two articulating surfaces is very low (0.02) [26-27]. Though hip prostheses have been successful in increasing mobility and decreasing pain, even the very best hip implant does not provide the low friction coefficient that are observed in healthy hip joints. Even the best artificial anti-friction materials are surpassed by the remarkable lubricating properties of joint cartilage [28].

Wear of the articulating components of hip implants is a major concern because it can decrease the integrity of the implant components. However, the wear debris that is produced can also diminish the life of the implant. Wear particles can also be generated from non-articulating modular junctions and the external surfaces of the implants [25]. Small particles of PMMA or bone can rub against external surfaces of the prosthesis and accelerate wear [29]. The abrasion of small particles against external surfaces is especially a concern for hip prostheses that utilize Ti-6Al-4V, which has poor tribological properties. The wear debris can compress against the bone and induce osteocyte death and necrosis or loosen particles of the implant by superficial abrasion [17]. Due to the important role of wear in the life of an implant, research examining the wear behavior of prosthesis components is essential in producing better hip prostheses.

2.4 SIGNIFICANCE OF CORROSION IN THR

Hip prostheses must endure prolonged exposure to the biological environment with minimum degradation and corrosion. The biological environment can be described as "an aqueous medium containing various anions, cations, organic substances, and dissolved oxygen [22]." Cations, such as Na^+, K^+, Mg^{2+}, and Ca^{2+} in addition to chloride, phosphate, and bicarbonate anions are commonly found in this environment [22]. The average pH in the body is 7.4, and a temperature around 37°C is maintained. A successful hip implant should be made of materials that can survive in this environment with the least amount of degradation and adverse reactions to the body.

In a hip prosthesis, the metal component is most susceptible to corrosion in the biological environment [22]. Even corrosion resistant metals will experience some deterioration after prolonged exposure to the environment. The following corrosion related concerns [22] must be considered:

- What is the corrosion behavior of the metal in the biological environment?
- How does the corrosion behavior change with variations in the biological environment?
- How does mechanical stress influence the corrosion behavior?
- How do the corrosion products affect the body?

Finding metals that address all the given corrosion considerations are difficult. Usually, the most noble metals (e.g., Au and Pt) that have the best corrosion resistances are rarely used in hip implants because they have inferior mechanical properties. Therefore, the challenge of material selection for hip prostheses components is finding materials that can withstand the corrosive environments of the body but still possess the mechanical properties that are required to successfully function in the hip joint.

CHAPTER 3: LITERATURE REVIEW

3.1 BASIC PRINCIPLES OF TRIBOLOGY

3.1.1 Definition and Types of Wear

Tribology is defined as "the science and technology of interacting surfaces in relative motion and of practices related thereto" and is associated with friction, lubrication, and wear [30]. Tribology has immense economic significance because tribological problems account for several percent of the gross national product [31]. Therefore, tribology affects a broad spectrum of industries. A significant area of tribological research includes efforts to improve wear behavior of human artificial joints to extend service life [32]. Wear is broadly defined as damage to a solid surface due to relative motion between the surface and a contacting substance or substances [30]. Some of the various categories of wear are adhesive wear, fatigue wear, corrosion wear, and abrasive wear.

Adhesive wear is defined as the material loss "when two nominally flat solid bodies are in sliding contact, whether lubricated or not" [33-35]. Bonding of the solid bodies is said to occur at the asperity contacts. These contacts may be detached from the surface due to the shearing caused by sliding. The fragments may be transferred back to the original surface or become wear debris [34].

Fatigue wear can be categorized as subsurface or surface wear. The former is a consequence of repeated rolling, and the later, a result of repeated sliding [34]. The unloading and loading will eventually cause spalling, separation of particles in the form of flakes. These fragments will leave pits on the surface. Thousands or millions of cycles must take place before this phenomena occurs. Therefore, fatigue wear is usually not as much of a concern as other modes of wear.

Corrosive (chemical) wear is the loss of material by both corrosion and sliding. Corrosive wear is described as a synergistic process because the damage done by corrosive wear is far more than the addition of the individual effects [36]. Due to the corrosive environment, an oxide film will form on the surface of the material. However, the sliding action wears the protective film away and allows for a more rapid chemical attack [34].

Abrasive wear is defined as the movement of hard particles or protuberances along a solid surface that generally involves the progressive loss of material [32-33]. Abrasion is characterized as either two-body or three-body wear. Two-body wear is defined as an abrasive sliding along a surface, where the abrasive is generally defined as the harder surface [32-34]. Three body wear is characterized by an abrasive being caught between two other surfaces [32-34]. Two-body systems generally experience more severe wear than three-body systems [32-33]. Processes that can remove material in abrasion are plowing, wedge formation, and cutting [34]. Due to the complexity of abrasion, deformation is generally a combination of these mechanisms. Abrasive wear of Ti-6Al-

4V is a significant concern in hip prostheses due to the abrasion by small particles of PMMA or bone [29].

3.1.2 Wear Test Methods

Wear screening tests provide an inexpensive and fast method to rank materials being considered for tribological applications. After the candidates have been ranked, the top materials are subjected to more complicated tests that better simulate the application environment. By accelerating wear, these tests are able to provide a rough estimate of the degradation expected during a specified time period of service.

The accelerated test apparatuses can control such factors as applied load, sliding velocity, and sample geometry. Some of the most common wear-testing geometries for screening materials are shown in Figure 4. The most commonly used test apparatus during the development of materials for tribological applications is the pin-on-disk wear test (Figure 4a). The pin-on-disk wear test is an in-vitro screening test commonly used for materials being considered for replacement implants. During this test, the pin is held stationary and the disk rotates. Possible geometries for the pin are a nonrotating ball, a hemispherically tipped rider, a rectangular parallelepiped, or a flat-ended cylinder [34].

Pin-on-disk wear tests can compare the wear resistances of materials by comparing their wear factors. During a pin-on-disk wear test, the maximum volume of wear, V, can be given by:

$$V = Ad \tag{1}$$

where A is the cross-sectional area of the groove due to the pin, and d is the sliding distance. A is dependent on the shape of the pin and can be written as

$$A = k_1 p \tag{2}$$

where k is a constant dependent on the shape, and p is the depth of penetration. The penetration can be related to the load, L, and hardness, H, of the material by the following equation:

$$p = k_2 L/H \tag{3}$$

where k_2 is another shape constant. The combination of equations 1-3 results in an expression for the wear factor.

$$k = \frac{VH}{Ld} \tag{4}$$

Equation 4 is referred to as the Archard wear law, and k is referred to as the wear coefficient or the wear factor [30, 32].

3.1.3 Types of Wear Measurements

There are various approaches to determining amounts of wear. The approach taken can depend on factors such as amount of wear, accuracy needed, and irregularity of the worn surface. Ruff [37] categorizes wear measurements as mass loss measurements, linear measurements, volume measurements, and area measurements.

Mass loss measurements are the most straightforward for wear damage that results in a substantial loss of material. The specimen is weighed before and after wear exposure. The difference in mass represents the mass of material that was loss due to wear. The specimens must be cleaned properly to avoid extraneous matter on the surface that could lead to inaccurate weight measurements. Difficulties with this technique occur as the parts involved become smaller and lighter or the material loss becomes smaller [37]. Also, plastically displaced material is not accounted for in the weight difference [37]. The amount of wear is commonly expressed in either mass loss or rate of mass loss. However, ASTM wear standards recommend converting mass loss to volume loss so that materials of different densities can be compared.

Another technique for quantifying the loss of material is to measure dimensional change. This type of measurement is common when there is a set tolerance on the loss of dimension before the integrity of a system is lost. Wear of shafts and piston cylinder walls are examples. ASTM Standard G 99 provides an outline of measuring dimensional change in the pin length and gives geometric relations to convert the wear scar size to wear volume.

Volume measures of wear are commonly used when the worn region has an irregular or unsymmetrical shape. In these cases, the worn surface is traced with an X-Y stylus profiling system, and three-dimensional images can be generated. This technique is also beneficial when there is localized material adhesion [37].

Area measures of wear are convenient when wear contact geometries produce material loss over a localized area. This type of measurement is most relevant to this research because it is commonly used in determination of wear loss in pin-on flat (reciprocating) test and pin-on-disk test. The amount of wear can be measured by determining the surface profile of the wear track perpendicular to the sliding direction. An example surface profile perpendicular to the wear track is illustrated in Figure 5. Note that the figure shows ridges of material on both sides of the wear track due to plastic deformation. This displaced material is usually ignored in the wear calculations [37]. Numerical integration of the profile gives the cross-sectional area of the wear track. This information can be used to calculate the amount of wear per length of the wear track [37].

3.1.4 Tribological Behavior of Ti-6Al-4V and Other Ti alloys

Titanium alloys have an attractive quality of high strength to weight ratio. Titanium alloys also have high toughness and corrosion resistance making them practical for

biomedical prosthesis devices. However, these alloys have poor surface hardness and wear resistance [38-41]. Nevertheless, Ti-6Al-4V is commonly used as a load bearing bio-implant material [42]. Surface modifications have been examined as a means to improve the tribological behavior of Ti-6Al-4V. Vapor deposition and thermochemical conversion are two common surface modification processes used to improve the wear resistance of Ti-6Al-4V components in hip replacement implants [38].

Vapor Deposition Processes. Vapor deposition processes can be categorized as chemical vapor deposition (CVD) or physical vapor deposition (PVD). CVD is deposition of a solid material from the vapor phase onto a heated substrate [43]. In PVD, material vapors are created via evaporation, sputtering, or laser ablation. The film is then deposited on the substrate by condensation. Physical vapor deposition techniques are more prevalent in surface modification of Ti-6Al-4V than chemical vapor deposition methods. Physical vapor deposition processes include plasma sprays, evaporation, sputtering, and ion implantation. Ion implantation has been the most common PVD method in the literature used to reduce Ti-6Al-4V wear debris [44]. This technique was pioneered by Williams and Buchanan [45-52].

Ion implantation involves the creation of a charged particle in an ion source. The ions are accelerated at high velocities and directed at the substrate, "where the ions dissipate their energy and come to rest by colliding with substrate atoms [53]." The implanted atoms and the defects in the substrate from the collision alter the mechanical properties of the surface.

In research conducted by Torregrosa et al. [54], aims were made at improving the wear behavior of Ti-6Al-4V sliding against UHMWPE by nitrogen ion implantation. Reciprocation pin-on-disk wear tests were performed on unmodified Ti-6Al-4V and Ti-6Al-4V with implant doses of 2×10^{17} and 5×10^{17} N^+ cm^{-2}. The surface treatment was found to decrease the wear rate by a factor ranging from 2 to 7. Similarly, Itoh et al. [55] examined the tribological properties of N^{2+}-ion implantation of Ti-6Al-4V by performing lubricated ball-on-disk tests against steel balls. It was found that N^{2+}-ion implantation significantly reduced the volumetric wear of the Ti-6Al-4V disks as well as the steel balls. The study showed that increases in ion doses did lead to increases in Knoop hardness. However, implantation did not monotonically improve the tribological properties with increasing dosage, which suggests that wear resistance depends on surface hardness and surface structure [55].

Schmidt et al. examined how ion implantation of various elements (C, N, O, Y, Hf, Pt, Au) affects the wear behavior of Ti-6Al-4V [29]. Wear tests were performed with Ti-6Al-4V disks against PMMA pins. The microhardness of the Ti-6Al-4V disks was also examined as a function of species implanted. Ion-implantation provided microhardness that was higher than the non-implanted Ti-6Al-4V alloy with the nitrogen ion-implanted disk having the highest hardness. The wear resistance of Ti-6Al-4V against PMMA was shown to increase with microhardness [29].

Thermochemical Conversion Processes. Thermochemical conversion processes utilize thermal diffusion to modify the surface of a substrate. The most common thermochemical conversion surface treatments are nitriding, carburizing, and nitrocarburizing [38]. Nitriding is commonly mentioned in the literature as means to improve the wear properties of Ti alloys being considered for implants. This process offers the advantage of a deeper modified layer. The simplest way to achieve nitriding is to place the substrate in a nitrogen rich furnace. Gaseous ammonia can be a source of nitrogen for nitriding. When dealing with Ti alloys, furnace temperatures above 900°C can lead to the adverse effect of irreversible grain growth [38]. However, salt baths and plasma-assisted processes are just a few alternatives that also achieve nitriding [56-57].

Yilbas et al. investigated the tribological and mechanical properties of plasma-nitrided Ti-6Al-4V [58]. Ball-on-disks wear tests were performed with a 3 mm ruby ball and an oil lubricant to investigate the wear behavior. The study confirmed that plasma nitriding did increase the wear resistance of Ti-6Al-4V. Rodriguez et al. conducted abrasive wear tests on Ti-6Al-4V and nitrided Ti-6Al-4V [59]. The experiments showed that the abrasive wear speed for the nitrided samples were about 75% lower than for unmodified Ti-6Al-4V samples.

Wear Behavior of Other Ti Alloys. As mentioned previously, biocompatibility concerns with Al and V [60-62] have led to searches for alternative Ti alloys to Ti-6Al-4V that will have better wear behavior and less toxicity concerns. β–Ti alloys, named because of a β (BCC) microstructure, have emerged because their compositions tend to eliminate at least Al or V. These alloys are also popular because they can be processed to higher strength levels and posses better notch properties and toughness than α(HCP) + β alloys (e.g., Ti-6Al-4V) [62]. Another advantage of β Ti alloys is their lower modulus, which can reduce the concerns of stress shielding. The wear behavior of β-Ti alloys has been investigated to determine if they exhibit better tribological characteristics than Ti-6Al-4V.

In a review paper that investigated the wear properties of various β-Ti alloys, Long et al. [44] concluded that the wear resistance of β-Ti alloys showed improvement when compared to Ti-6Al-4V. However, it was concluded that the composition of the surface oxide was a critical factor in the wear behavior of β alloys. In a similar study, Long et al. [41] examined the tribological behavior of three β alloys (Ti-35Nb-8Zr-5Ta, Ti-35Nb-8Zr-5Ta with increased oxygen, and Ti-15Mo). Reciprocating-sliding experiments against steel revealed that β alloys did not provide higher wear resistance when compared to Ti-6Al-4V. Other studies suggest that the wear properties of α + β titanium alloys are better than β titanium alloys. In the research conducted by Niinomi et al., pin-on disk experiments with an alumina ball in Ringer's solution showed that Ti-6Al-4V possessed higher wear resistance than Ti-15Mo, Ti-12Mo-6Zr-2Fe, Ti-16Nv-10Hf, and Ti-15Mo-3Zr-3Al, which are all β alloys [63]. Similarly, Khan et al. [64] conducted pin-on-disk wear tests with an alumina pin and concluded that Ti-6Al-4V was more wear resistant than Ti-13Nb-Zr and Ti-6Al-7Nb, both β type alloys. These wear experiments were

conducted in distilled water and protein containing solutions. The literature suggests that β titanium alloys do not consistently provide increased wear resistance when compared to Ti-6Al-4V.

3.2 BASIC PRINCIPLES OF CORROSION

Corrosion is defined as the deterioration of materials due to reactions with their environment [65]. Examples of corrosion are anything from rusting of steel in water to the current subject of corrosion of metallic surgical implant materials. In general, corrosion is considered a surface phenomenon where the mechanisms are atomic, molecular, or ionic transport processes that occur at the material/environment interface [22, 65]. These transport processes can be considered as electrochemical, chemical, or physical. Electrochemical corrosion is the release of ions into the environment, and the movement of electrons in the material. Electrochemical corrosion will be focused on in this study due to its correlation with the corrosion of metals in a biological solution [65].

Electrochemical corrosion is probably best illustrated in the corrosion of metal in an aqueous solution. Atoms at the interface of the metal go into solution as ions and electrons migrate to a separate site to sustain the reaction [65]. Figure 6 illustrates the uniform corrosion of a metal in an aerated neutral or alkaline electrolyte. The following equation expresses the chemical reaction occurring:

$$M + \frac{m}{4}O_2 + \frac{m}{2}H_2O \rightarrow M^{m+} + mOH^- \qquad (5)$$

where M is an unspecified metal and m is the metal valence. This chemical reaction can be separated into anodic and cathodic reactions. The anodic reaction, which involves oxidation, loss of electrons of the metal, is given below.

$$M \rightarrow M^{m+} + me^- \qquad (6)$$

The cathodic reaction depends on the nature of the electrolyte. However, the two most important cathodic reactions in aerated aqueous solutions are the reduction of dissolved oxygen:

$$\frac{m}{4}O_2 + \frac{m}{2}H_2O + me^- \rightarrow mOH^- \qquad (7)$$

and the direct reduction of water:

$$mH_2O + me^- \rightarrow \frac{m}{2}H_2 + mOH^- \qquad (8)$$

The cathodic reactions involve processes by which electrons are consumed. Both cathodic reactions contribute to the consummation of electrons. However, at higher

potentials the reduction of oxygen dominates. The direct reduction of water dominates at lower potentials.

3.2.1 The Electrochemical Corrosion Circuit

The concept of aqueous corrosion that is illustrated in Figure 6 can also be represented by an electrochemical cell consisting of two half cells [65]. Figure 7 is a schematic of the elementary electrochemical corrosion circuit. The area on the metal where there is a net loss of electrons ($M \rightarrow M^{m+} + me$) is defined as the anodic site, A_a. The cathodic site, A_c, defines the area where there is net consumption of electrons ($X^{x+} + xe \rightarrow X$). Due to the transfer of electrons, there are differences in electrical potentials over the anodic and cathodic sites, $\Delta\phi_a$ and $\Delta\phi_c$, respectively [65]. When these potential differences are expressed relative to the standard hydrogen reference electrode, $\Delta\phi_a$ is expressed as E_M and $\Delta\phi_c$ as E_X.

Figure 7 illustrates that in the metal there is a net movement of electrons from the anodic site to the cathodic site. Since conventional current is defined by the movement of positive charges, current in the metal flows in the opposite direction of the electrons. In the solution, current flows from the anodic site to the cathodic site. The driving force for the current in the solution is the potential difference in the solution, $\Delta\phi_S$, given by

$$\Delta\phi_S = \Delta\phi_c - \Delta\phi_a = E_X - E_M \qquad (9)$$

Using Ohm's Law, the corrosion current, I_{corr}, can be expressed in the following manner

$$I_{corr} = (E_X - E_M) \Big/ \left(\sum_i^n R_i \right) \qquad (10)$$

where $\sum R$ represents various resistances associated with the system such as the resistances of the solution, metal, and interface. Dividing the corrosion current by the anodic area, the anodic current density is obtained. The anodic current density, i_{corr}, is a useful quantity because with Faraday's Law it can be used to predict the corrosion intensity (CI), mass loss per unit time per unit area, or corrosion penetration rate (CPR), linear dimension loss per unit time. The expressions for CI and CPR are given below

$$CI\left(g/\left(m^2 y\right)\right) = 0.327\, Mi_{corr}/m \qquad (11)$$

$$CPR(\mu m/y) = 0.327\, Mi_{corr}/m\rho \qquad (12)$$

where M is the atomic mass in g/mol, m is the valence, ρ is the density in g/cm^3, and i_{corr} is the current density in mA/m^2 [65].

The current density is also an important quantity because it is directly related to the interfacial potential. When the current density has a linear relationship to the potential, it is said to exhibit Tafel behavior. However, a large number of metals have potential and current densities that have a nonlinear relationship called active-passive behavior. For active-passive metals, precipitation occurs at the metal-solution interface when a critical concentration of metal ions passes into solution [65]. This solid corrosion product can decrease corrosion if it is stable and adherent. This paper will concentrate on active-passive behavior, since Ti-alloys exhibit this behavior. Active-passive behavior will be discussed later in further detail.

3.2.2 Electrochemical Corrosion-Rate Measurements

Electrochemical experiments provide a relatively simple way to observe the corrosion behavior of the material and calculate corrosion rates. These electrochemical experiments commonly use a potentiostatic circuit as shown in Figure 8 [65]. The working electrode (WE) is the material being studied, the corrosion sample. The counter electrode (CE) supports oxidation or reduction reactions. The counter electrode is made of materials, such as graphite or platinum, that will conduct electrons without corroding and contaminating the electrolyte [65]. The potential of the WE is measured relative to the reference electrode (RE) by an electrometer. The potentiostat is able to maintain a constant potential between the WE and RE even though there may be large changes in the external current, I_{ex} [65]:

$$I_{ex} = I_{ox,m} - I_{red,x} \qquad (13)$$

where $I_{ox,\,m}$ is the oxidation current at the metal surface, and $I_{red,\,x}$ is the cathodic current at the metal surface. When there is no external current,

$$I_{ex} = 0 \;\therefore\; I_{ox,m} = I_{red,x} \qquad (14)$$

and the sample is said to be freely corroding. The potential that corresponds to $I_{ex} = 0$ is the corrosion potential, E_{corr}, (open-circuit potential). E_{corr} varies with pH, oxygen concentration, and concentrations of other species capable of undergoing oxidation/reduction reactions. The open-circuit potential represents the potential at which the net oxidation reaction equals the net reduction reaction.

In an electrochemical polarization experiment, the WE is polarized from E_{corr} so its corrosion behavior can be observed. Before an electrochemical polarization experiment, the sample is allowed to stabilize in the solution until E_{corr} does not change more than 1 mV for a 5-minute time span. The potential is the controlled parameter, and the external current is measured during these experiments. When the potentiostat is set to polarize the WE anodically, the potential is increased relative to E_{corr}; thus, the net reaction on the WE is oxidation (i.e., $I_{ox,\,m} > I_{red,\,x}$). When the potential is decreased relative to E_{corr}, the WE is being cathodically polarized ($I_{red,\,x} > I_{ox,\,m}$).

By polarizing the WE anodically and cathodically, anodic and cathodic parts of the polarization curve can be obtained, respectively. Figure 9 represents a schematic experimental polarization curve of an active-passive metal. E_{corr} is the value that both the anodic and cathodic parts of the curve asymptotically approach, which signifies $I_{ex} = 0$. I_{corr} is the corrosion current that corresponds to E_{corr}. At E_{corr} the following is true

$$I_{ox,m} = I_{red,x} \;\therefore\; I_{corr} = I_{ox,m} = I_{red,x} \tag{15}$$

Thus, I_{corr} graphically is the current that corresponds to the intercept of E_{corr} and the extrapolation of the cathodic curve.

In this research, the polarization-resistance, or Stern-Geary, method was used to obtain i_{corr}. This method is based on the following equation:

$$\left(\frac{dE}{di_{ex}}\right)_{E_{corr}} = R_p = \frac{\beta_{ox,m}\beta_{red,x}}{2.3\, i_{corr}\left(\beta_{ox,m} + \beta_{red,x}\right)} \tag{16}$$

where R_p is the polarization resistance and is in ohm-m^2 and $\beta_{ox,m}$ and $\beta_{red,x}$ are Tafel constants related to the experimental curve and are expressed in mV. R_p represents the slope of the experimental E versus i_{ex} curve at E_{corr}. Rearranging equation 16 yields the following equation:

$$i_{corr} = \frac{\beta_{ox,m}\beta_{red,x}}{2.3R_p\left(\beta_{ox,m} + \beta_{red,x}\right)} \tag{17}$$

If $\beta_{ox,m}$ and $\beta_{red,x}$ are approximated to be 100 mV, equation 17 is transformed into the a more familiar form:

$$i_{corr} = \frac{22mV}{R_p} \tag{18}$$

where R_p is obtained from experimental data. The polarization-resistance method provides an effective way to obtain i_{corr} thus providing an effective way to calculate corrosion rates. Other information that can be extracted from experimental polarization curves will be discussed in the next section.

3.2.3 Active-Passive Corrosion Behavior and Cyclic-Anodic Polarization Tests

Before cyclic-anodic polarization tests can be described, a more detailed explanation of active-passive behavior is required. Active-passive metals precipitate a solid corrosion product at the surface when a critical concentration of ions passes into solution. The

solid corrosion products can be hydroxides, oxides, sulfides, or mixtures of all of these [65]. If the corrosion product adheres to the metal and has a high resistance to electron ion transport, the corrosion rates can be significantly decreased. The decrease in corrosion due to the solid corrosion product, or passive film, is referred to as passivation. Figure 10 is a schematic representation of Tafel behavior and active-passive behavior. Tafel behavior shows an increase in corrosion at higher potentials (increasing the oxidizing power). Active-passive alloys will exhibit an increase in corrosion with an increase in potential initially. However, further increase in potential decreases the corrosion, which corresponds to the formation of the passive film. The passive film eventually is destroyed when it is no longer thermodynamically stable or when it breaks down locally, and corrosion rates rise again.

Cyclic-anodic polarization tests provide useful information about the anodic behavior of active-passive metals. The potentials at which the passive film is destroyed and reformed can be obtained from the cyclic experiments. With these tests, E_{corr} and i_{corr} can also be obtained. The cyclic-anodic polarization scans are usually started 50 mV below E_{corr} to obtain part of the cathodic curve (for extrapolation). The potential is increased until a preset current density is reached. Then the potential is reversed and decreases until the original potential is reached.

Figure 11 is a schematic of the possible paths of an active-passive alloy during a cyclic-anodic-polarization test. Path one illustrates a material that forms a passive film that dissipates because the film is not stable at E_{trans}. However, the film reforms when the potential scan is reversed. Paths two and three are examples of local breakdown in the passive film. Localized corrosion can be recognized in cyclic-anodic polarization tests because it is accompanied by a polarization loop [65]. The breakdown potential, E_{break}, represents the onset of localized corrosion. The local breakdown may be a result of pitting corrosion, E_{pit}, or crevice corrosion, E_{crev}. When the scan is reversed, the surface is completely repassivated at the protection potential, E_{prot}. When E_{prot} is above E_{corr} as in path 2, there will be no localized corrosion at natural corroding conditions, E_{corr}. If E_{prot} is below E_{corr} as in path 3, localized corrosion can occur at E_{corr} at surface flaws (e.g., scratches).

3.3 CORROSION OF TI-6AL-4V AND SIMILAR TI ALLOYS

Ti-6Al-4V has corrosion resistance that is superior to alternative biomaterials such as stainless steels and some cobalt-chromium alloys [66]. The formation of a stable TiO_2 film is the reason for the high corrosion resistance of Ti-6Al-4V is [65-67]. However, the passive film does not eliminate corrosion current; it just decreases the corrosion rates. Therefore, even with the existence of a stable passive film, ion release of metallic species still occurs in the body, which is of concern due to the presence of Al and V. This concern has fueled electrochemistry research on Ti alloys that have corrosion properties comparable to Ti-6Al-4V but with elements of lower toxicity than Al and V.

M. Khan et al. [66] compared the corrosion behavior of Ti-6Al-4V, Ti-6Al-7Nb, and Ti-14Nb-13Zr in a 37°C phosphate buffered saline (PBS), bovine albumin solution in PBS,

and 10% fetal calf serum in PBS solution. Cyclic-anodic polarization experiments were performed on the three alloys. The results in the PBS and bovine albumin solution in PBS will be emphasized because the pH of these solutions (7.4) is relevant to the environment of the body. The corrosion resistance of the alloys was expressed by the difference between E_{break} and E_{prot} with smaller differences indicating more resistance to localized corrosion. In the PBS solution, Ti-6Al-7Nb and Ti-14Nb-13Zr displayed higher corrosion resistances than Ti-6Al-4V. In the bovine albumin solution in PBS, Ti-6Al-4V illustrated the best corrosion resistance with Ti-14Nb-13Zr and Ti-6Al-7Nb following.

In a similar study, Lopez et al. [67] compared the corrosion behaviors of Ti-7Nb-6Al, Ti-13Nb-13Zr, and Ti-15Zr-Nb in Hank's solution. These results were compared to their past results of Ti-6Al-4V [68]. The i_{corr} values of Ti-13Nb-13Zr, Ti-7Nb-6Al, and Ti-15Zr-4Nb were 0.08, 0.09, and 0.1 mA/m^2, respectively. These values are significantly lower than the i_{corr} for Ti-6Al-4V, which was around 0.5 mA/m^2. Cyclic-anodic polarization tests were conducted to evaluate susceptibility to localized corrosion. Despite potentials up to 2000 mV, no E_{break} was observed for any of the alloys. An absence of E_{break} suggested that the surface remained passivated and only uniform corrosion occurred. Ti-7Nb-6Al showed the highest values of current density. However, Ti-13Nb-13Zr and Ti-15Zr-4Nb had very low passivation current densities ($\approx 10^{-1}$ mA/m^2). These passivation current densities were lower than that of Ti-6Al-4V (between 10^1 and 10^2 mA/m^2). The results suggested lower corrosion currents for Ti-13Nb-13Zr and Ti-15Zr-4Nb than for the conventional biomaterial Ti-6Al-4V.

Kuphasuk et al. [69] compared the corrosion behaviors of commercially pure titanium, Ti-5Al-2.5Fe, Ti-5Al-3Mo-4Zr, NiTi, and Ti-6Al-4V in a 37°C ringer solution. Cyclic-anodic polarization experiments were run on all of the alloys. Only NiTi experienced an E_{break}, 500 mV SCE. Commercially pure Ti and Ti-5Al-2.5Fe exhibited the lowest corrosion rates (0.012 ± 0.014 and 0.0200 ± 0.025 mpy, respectively). Ti-6Al-4V and NiTi had the highest corrosion rates with values of 0.0683 ± 0.088 and 0.0707 ± 0.090 mpy, respectively. In a similar study, Aziz-Kerrzo et al. [70] investigated the anodic polarization behavior of Ti, Ti-6Al-4V, and Ti-45 Ni in a buffered saline solution. This study also illustrated that Ti and Ti-6Al-4V were not susceptible to localized corrosion. Ti had a consistent passive current density of the order of 20-30 mA/m^2 even at potentials higher than 1600 mV SCE. Ti-6Al-4V had anodic current density that reached values approximately 200 mA/m^2 at 1000 mV SCE. The electrochemical behavior of Ti-45Ni was similar to that reported by Kuphasuk et al. Ti-45Ni was found to be susceptible to pitting corrosion with E_{break} ranging from 200 to 530 mV SCE.

CHAPTER 4: OBJECTIVES, MATERIALS, AND PROCEDURES

4.1 OBJECTIVES

A significant amount of biomaterial research has focused on improving the wear resistance of Ti-6Al-4V by surface modification, such as ion implantation and nitriding. Though these techniques generally have had a positive effect on the tribological behavior, they do not address the long-term biocompatibility concerns of aluminum and vanadium [44, 53, 66-69, 71]. Attempts to create β–Ti alloys that contain β stabilizers (e.g. Nb, Ta, and Mo) have been successful in eliminating Al and V. However, the β-alloys have wear properties that are the same or inferior to that Ti-6Al-4V. In this research, the wear resistance of Ti-6Al-4V and heat-treated Ti-8Mo are compared. The objective is to determine if the heat-treated Ti-8Mo will provide better wear resistance than Ti-6Al-4V.

The corrosion behavior of Ti-6Al-4V and Ti-8Mo will also be compared using cyclic-anodic polarization tests. Titanium alloys are known for their excellent corrosion resistance. Ti-6Al-4V has been shown to have excellent corrosion behavior with low passive currents and no localized corrosion. If Ti-8Mo has comparable corrosion resistance to Ti-6Al-4V and better wear resistance, it could be more seriously considered as a candidate for hip replacement implants.

4.2 MATERIALS

Titanium Industries, Inc. provided Ti-6Al-4V ELI plates following ASTM F136-96 specifications. The specimens were annealed at 732°C for 30 minutes to obtain a duplex ($\alpha + \beta$) structure. The grain size reported was ASTM 8.5. The Ti-6Al-4V ELI plates were machined at The University of Tennessee into flat disks, each with a thickness of 5.82 mm and inner/outer diameters of 8.00 and 31.22 mm, respectively.

The titanium-molybdenum alloy (Ti-8Mo [wt. %]) was manufactured at The University of Tennessee. The Ti-8Mo alloy was fabricated by arc melting in an inert argon atmosphere. The material was held at 925°C for 16 hours, immediately transferred to a furnace at 776°C and isothermally aged for 2 hours in the $\alpha + \beta$ region, then water quenched to room temperature. The specimens were heat treated in quartz tubing backfilled with a 0.25 argon atmosphere to prevent unwanted oxidation [1]. This heat treatment was performed as described by James and Moon [9] to obtain a microstructure of a precipitated ω phase in a $\alpha + \beta$ matrix. James and Moon demonstrated that the ω phase was associated with increases in hardness and strength, which inferred that the ω phase could lead to improved wear resistance. The Ti-8Mo flat disk has a thickness of 5.69 mm and inner/outer diameters of 8.02 and 27.56 mm, respectively.

4.3 EXPERIMENTAL PROCEDURES

4.3.1 Optical Microscopy

Both Ti-6Al-4V and Ti-8Mo were metallographically prepared to a 0.01 micron alumina slurry surface finish and etched with Kroll's reagent (94 mL H_20, 4 mL HNO_3, and 2 mL

HF). Observation by optical microscopy confirmed a duplex microstructure of α and β phases for Ti-6Al-4V. The microstructure of Ti-6Al-4V is shown in Figure 12. The light areas are the HCP, α phase. The β phase, which is represented by the dark areas, has a BCC structure. Vanadium stabilizes the β phase while Al is a solid solution strengthener. Figure 13 is a micrograph of Ti-8Mo. The micrograph shows a structure of α and β phases. The ω phase is on the order of nanometers and cannot be resolved with an optical microscope.

4.3.2 Pin-on-Disk Wear/Potentiostatic Experiments

Pin-on-disk wear tests were performed on both the Ti-6Al-4V and Ti-8Mo samples with Polymethylmethacrylate (PMMA) pins to provide an effective way to rank their wear behavior. The wear of PMMA against the samples was to simulate the abrasion that a hip implant might experience due to bone-cement wear debris or bone. PMMA (Zimmer, Warsaw, IN) pins were prepared by mixing a prepolymerized powder and a liquid monomer and pressing into a mold. The PMMA pins were allowed to cure for 24 hours. The flat cylindrical PMMA pins were set into a "commercially pure" titanium threaded bit. This process was done by applying Quick Setting Epoxy Adhesive (Pacer Technology, Rancho Cucamonga, CA) to the tip of the PMMA pin and then inserting it into the titanium threaded bit. After drying for 24 hours, the titanium bit was mounted onto the arm of the wear test machine. The diameter of the PMMA pin was approximately 1.6 mm (1/16 inch).

Before each test, the pin was prepared to a 600-grit SiC finish, and the disk was prepared to a 0.01 micron alumina surface finish. All surfaces except the wear surfaces were coated with insulating enamel. Once the enamel was dried, a bovine serum test solution was prepared. The serum, which was meant to simulate the synovial fluid of human joints, was prepared by mixing 230 mL of bovine serum (Sigma Chemical Co., St Louis, MO), 350 mL distilled water, 58 mL of disodium ehylenediamine tetra-acetate (EDTA), and 1.28 g of sodium azide (NaN_3). The EDTA (Lab Chem Inc., Pittsburgh, PA) is added to prevent degradation in the solution, and the NaN_3 acted as a disinfectant. The solution was poured into a 600 mL beaker and placed on the base of the wear test machine (Figure 14).

The disk sample was screwed into the middle of the wear test machine and then the corrosion cell was lowered until the sample was completely immersed in the serum. The pin was placed on the circular disk sample at a designated radius and was also submerged in the solution.

The contact stress was approximately 3.4 MPa (500 psi) when the lead weight was suspended from the hook; 98.75 g of lead shot was added to the cup closest to the pin, and 21.42 g of lead shot is added to the cup on the right. The specified stress was designed to simulate the average contact stress experienced in a typical hip implant [54]. The weight in the two cups on the arm was to insure that the normal force was being generated by the suspended weight. The testing machine rotated the disk at a rotational velocity of 150 mm/s. The wear track radius was determined to be 12 mm. The wear

tests were run for 24 hours with the previously discussed parameters to simulate 1 year of in vivo use. The testing conditions of the samples and the amount of time the test was run reproduces the 10.7 km of interfacial sliding the average artificial hip implant experiences per year [72-73].

A potentiostat was used to monitor the current during the wear testing. In the three-electrode corrosion set-up, the titanium wear samples were the working electrodes, the platinum was the counter electrode, and a saturated calomel electrode (SCE) was the reference electrode. The sample was allowed to stabilize until the corrosion potential (E_{corr}) did not change by more than 1 mV in a 5-minute time span. After E_{corr} stabilized, a constant potential 100 mV higher than E_{corr} was applied, and the anodic current was measured as a function of time.

4.3.3 Profilometry

The mass loss, or wear of the samples, was determined by area measures of wear. A profilometer was used to make surface profiles of the wear track, perpendicular to the sliding direction. Four profilometry scans were conducted on each sample (approximately 90 degrees apart). The numerical integration of the surface profiles via a MATLAB program (see *Appendix of MATLAB Code*) written by Christopher Stephens gave the cross-sectional area of the wear track and led to a determination of the amount of wear per unit length of the sliding contact. The program fit an equation to the wear surface using the profilometry data (ignoring the data associated with the wear track). The program then calculated the difference between the y-values (height) of the equation (at a specified x-value) and the y-values from the profilometry data that corresponded to the same specified value of x (distance along the sample). This difference represents the depth of the wear track and was used in for numerical integration. All profilometry was performed at Oak Ridge National Laboratory on a Taylor Hobson Talysurf 10 profilometer through collaborations with Drs. Peter Blau and Ron Ott.

4.3.4 Cyclic-Anodic Polarization Tests

Electrochemical cyclic-anodic-polarization tests were conducted on each sample using an EG&G Princeton Applied Research Model 263A Potentiostat/Galvanostat with EG&G 352 SoftCorr III computer software. The electrochemical cell consisted of the working electrode, a saturated calomel reference electrode, a platinum counter electrode, and the electrolyte. The biological environment was adapted from the procedure described by Hiromoto et al. [74]. The electrolyte was a phosphate buffered saline (PBS) solution (Table 2) at a temperature of 37°C. The oxygen concentration was controlled by aerating a N_2 gas mixture containing 0.4 % O_2. The flow rate of the gas mixture was approximately 50 mL/min. Before each polarization scan, the corrosion sample was allowed to stabilize in the electrolyte for 1 h or until the open-circuit corrosion potential, E_{corr}, changed by no more than 1 mV over a 5-minute time span. The starting potential was 50 mV below E_{corr} and continued in the positive direction until an anodic current density of 10^4 mA/m^2 was reached. When the specified anodic current density was attained, the scan direction is reversed and continued until the original potential was reached. The scan rate for all the polarization tests was 0.17 mV/s.

CHAPTER 5: RESULTS, CONCLUSIONS, AND RECOMMENDATIONS

5.1 WEAR RESULTS AND DISCUSSION

Five pin-on-disk wear tests were performed on both Ti-6Al-4V and Ti-8Mo. Figures 15 and 16 are representative surface profiles of Ti-6Al-4V and Ti-8Mo, respectively after pin-on-disks wear tests. The figures illustrate that Ti-6Al-4V experiences much more wear than Ti-8Mo. The representative profile for Ti-6Al-4V shows that there are portions of the wear track that are deeper than 30 microns. The profile for Ti-8Mo demonstrates little wear of the surface. The deepest portion of the track is around 15 microns. The data used to generate the surface profiles was analyzed via a MATLAB program. The MATLAB program calculated the area removed, A. Using the area value, the total volume lost by the sample was calculated using the following equation:

$$V = A[2\pi(R_O - R_I)] \qquad (19)$$

where V is the volume lost by the sample, R_O is the outside radius measured from the center of the sample, and R_I is the inside radius of the wear track measured from the center of the sample. After the volume lost was calculated, the mass loss was determined using the equation below:

$$TML = V \text{ x } \rho \qquad (20)$$

where TML is the total mass loss and ρ is the density of the sample.
Not only is there mass loss due the wear but also there is mass loss due to corrosion of the sample. The mass loss due to corrosion was calculated using the corrosion intensity. The corrosion intensity, CI, was calculated with the equation below.

$$CI(g / yr) = \frac{0.327 \text{ x } W \text{ x } I}{m} \qquad (21)$$

where W is the atomic weight (g/mol), I is the measured anodic current (mμA), and m is the valence of a titanium ion, which is 4. The mass loss due to corrosion, ML_{corr}, is calculated using the equation below.

$$ML_{corr} = (CI) \text{ x } t \qquad (22)$$

where t is the time of the test. The mass loss due to wear, ML_{wear}, is the difference between TML and ML_{corr}.

The average TML values for Ti-6Al-4V and Ti-8Mo were 1.6×10^{-3} and 1.5×10^{-4} g, respectively. The total mass loss of Ti-6Al-4V was more than 10 times that of Ti-8Mo.

Table 3 gives average values of mass loss for Ti-6Al-4V and Ti-8Mo. The table shows that the material loss due to wear for Ti-6Al-4V was greater than 10 times that of Ti-8Mo. The significantly lower values of material lost for Ti-8Mo supports that it has superior wear resistance to Ti-6Al-4V. The amount of material lost due to corrosion was significantly lower than that lost due to wear for both materials.

5.2 CORROSION RESULTS AND DISCUSSION

Cyclic-anodic-polarization curves of Ti-6Al-4V are shown in Figures 17 and 18, and cyclic-anodic-polarization curves of Ti-8Mo are shown in Figures 19 and 20. Four polarization scans were conducted on each alloy so that the average behavior of the alloy could be observed. The corrosion current densities were obtained using the polarization-resistance method.

Figure 17 shows scans on separate plots so their behavior could be more easily observed. Figure 18 plots all scans of Ti-6Al-4V on one plot. Examination of the corrosion surface after each test revealed no pits on the surface indicating that no localized corrosion occurred. All cyclic-anodic polarization curves possessed down-scans that exhibited lower current densities than the up-scans (i.e. no anodic loops). An absence of an anodic loop further supports that Ti-6Al-4V is shown to be resistant to localized corrosion over the tested potential range. All tests support that Ti-6Al-4V is resistant to localized corrosion at potentials exceeding 2000 mV. The average open-circuit potential, E_{corr}, of Ti-6Al-4V was -432 mV (SCE). The average corrosion current density, i_{corr}, that occurred at E_{corr} was 0.4 mA/m^2. Ti-6Al-4V showed passive current densities ranging from 6.5 to 7.0 mA/m^2. However, the vertical passive region of Ti-6Al-4V endures for about 850 mV and then there was a steady increase of current density with increasing potentials. This steady increase could have been associated with the oxidation of water ($H_2O \rightarrow O_2 + 4H^+ + 4e$) at higher potentials.

Figure 19 shows the cyclic-anodic-polarization behavior exhibited by Ti-8Mo in 2 of the four scans. After careful examination of the corrosion surface of Ti-8Mo, no pits were observed. Furthermore, none of the Ti-8Mo scans included an anodic loop. Each Ti-8Mo test reached potentials of over 2500 mV with no breakdown of the passive film. The average open-circuit potential and corrosion current density of Ti-8Mo is –274 mV (SCE) and 1.3 mA/m^2, respectively. The passive current density range was about 10 to 60 mA/m^2.

Table 4 contains i_{corr} and CPR values for all four scans for each alloy with average values. Figure 21 illustrates representative curves of Ti-6Al-4V and Ti-8Mo. Both Ti-6Al-4V and Ti-8Mo are extremely resistant to localized corrosion. The average passive current densities for Ti-6Al-4V and Ti-8Mo are 7 and 35 mA/m^2, respectively. The corrosion current densities and corrosion penetration rates, CPR, of Ti-6Al-4V and Ti-8Mo were 0.4 mA/m^2 and 0.3 um/y, respectively, for Ti-6Al-4V and 1.3 mA/m^2 and 1.1 um/y, respectively, for Ti-8Mo. Both of CPR values are very low and imply excellent resistance to uniform corrosion at natural corroding conditions.

5.3 CONCLUSIONS

This study examined the wear and corrosion behavior of Ti-6Al-4V ELI and a heat treated Ti-8Mo. The heat treated Ti-8Mo could provide a new alternative to Ti-6Al-4V as the material for femoral components of hip prostheses. Pin-on-disk wear experiments and electrochemical cyclic-anodic-polarization experiments in biological environments were performed on both alloys.

1. Pin-on-disk wear tests with PMMA pins were performed on Ti-6Al-4V and Ti-8Mo in a bovine serum, simulation of synovial fluid, at room temperature. The contact stress of the pin was 3.4 MPa with an interfacial velocity of 150 mm/s. The wear profiles show a significant difference in the wear properties of Ti-6Al-4V and Ti-8Mo. Ti-6Al-4V wear depths exceeded 30 microns while those of Ti-8Mo did not exceed 15 microns.
2. The average total mass loss values for Ti-6Al-4V and Ti-8Mo was 1.6×10^{-3} and 1.5×10^{-4} g, respectively. The total mass loss of Ti-6Al-4V was more than 10 times that of Ti-8Mo.
3. The average mass loss value due to wear for Ti-6Al-4V was greater than 10 times that of Ti-8Mo. For both alloys, the amount of material loss due to corrosion was significantly lower than that lost due to wear.
4. Cyclic-anodic-polarization experiments were conducted in a phosphate buffered saline (PBS) solution at 37°C. The oxygen concentration of the solution was controlled by aerating the solution with a N_2 gas mixture containing 0.4 % O_2. The flow rate of the gas mixture was approximately 50 mL/min. Both Ti-6Al-4V and Ti-8Mo were found to be extremely resistant to localized corrosion in the biological simulated environment.
5. Both alloys exhibited low corrosion current densities and low corrosion penetration rates. The corrosion currents and corrosion penetration rates, CPR, of Ti-6Al-4V and Ti-8Mo were 0.4 mA/m^2 and 0.3 um/y, respectively, for Ti-6Al-4V and 1.3 mA/m^2 and 1.1 μm/y, respectively, for Ti-8Mo.

5.4 RECOMMENDATIONS FOR ADDITIONAL RESEARCH

Some recommendations for future research in this area are as follows:

- Fabrication of additional Ti-8Mo via the procedure outlined in section 4.2.
- Additional pin-on-disk wear/potentiostatic tests on Ti-8Mo and Ti-6Al-4V in a bovine serum.
- Additional cyclic-anodic-polarization experiments on Ti-8Mo and Ti-6Al-4V in a PBS solution at 37°C.
- Mechanical testing (i.e. tensile and fatigue testing) of Ti-8Mo and Ti-6Al-4V to determine the modulus and fatigue life of Ti-8Mo and to verify the modulus and fatigue life of Ti-6Al-4V that have been reported in the literature.
- In vitro assessment of the tissue compatibility of Ti-8Mo and Ti-6Al-4V by utilizing cell culture assays (e.g., a direct contact test using L-929 mouse fibroblast cells).

LIST OF REFERENCES

1. P. Mainor, "Titanium-Molybdenum Alloys for Orthopedic Applications," Technical Review provided by the Materials Science and Engineering Department at The University of Tennessee, Knoxville, 1999.
2. K. Wang, The use of titanium for medical applications in the USA, *Mater. Sci. and Eng.*, vol. A213, 1996, p 134-137
3. R.T. Bothe, L.E. Beaton, and H.A. Davenport, "Reaction of bone to multiple metallic implants," *Surg. Gynecol. Obstet.*, Vol 71, 1940, p 598-602.
4. D.F. Williams, *Biocompatibility in Clinical Practice, Volume II*, CRC Press, Inc., 1981.
5. G.S. Leventhal, *J. Bone Joint Surg.*, Vol 33A (2), 1951, p 473
6. Slanina, W. Frech, A. Bernhardson, A. Cedegren and P. Mattsson, Influence of dietary factors on aluminum adsorption and retention in brain and bone of rat, *Acta Pharmacol. Toxicol.*, vol. 56, pp. 331-336, 1985.
7. G.B. van der Voet, E. Marani, S. Tio and F.A. De Wolff, "Aluminum neurotoxicity," in *Histo and Cyto-Chemistry as a Tool in Environmental Toxicology*, W. Graumann and J. Drukker, Eds. Fisher, Stuttgart, 1991, pp.?5-242.
8. R.L. Buly, "Titanium wear debris in failed cemented total hip arthroplasty," *J. Arthroplasty*, vol. 3 (3), 1992, pp. 315-325.
9. D.W. James and D.M. Moon, "The martensitic transformation in titanium binary alloys and its effect on mechanical properties," in The Science, Technology, and Applications of Titanium, R.I. Jaffee and H.M. Burte, Eds., Plenum Press, New York, 1973.
10. W.F. Ho, C.P. Ju, and J.H. Chern Lin, "Structure and properties of cast binary Ti-Mo alloys," *Biomaterials*, Vol. 20, 1999, pp. 2115-2122.
11. D. Kuroda, M. Niinomi, M. Morinaga, Y. Kato, and T. Yashiro, "Design and mechanical properties of new β type titanium alloys for implant materials," *Mater. Sci. Eng.*, vol. A243, 1998, pp. 244-249.
12. M. Niinomi, "Recent biocompatible metallic materials," in Structural Biomaterials for the 21st Century, M. Niinomi, T. Okabe, E.M. Taleff, D.R. Lesuer, and H.E. Lippard, Eds. TMS, 2001.
13. R.L.W. Messer and L.C. Lucas, "Evaluations of metabolic activities as biocompatibility tools: a study of individual ions' effects on fibroblasts," *Dent. Mater.*, Vol. 15, 1999, pp. 1-6.
14. W. Geursten, "Biocompatibility of dental casting alloys," *Crit Rev Oral Biol Med*, Vol. 13(1), 2002, pp. 71-84.
15. L.D. Zardiackas, D.W. Mitchell, and J.A. Disegi, "Characterization of Ti-15Mo beta titanium alloy for orthopaedic implant applications," in *Medical Application of Titanium and Its Alloys: The Material and Biological Issues, ASTM STP 1272*, S.A. Brown and J.E. Lemons, Eds., ASTM, 1996.
16. K. Hardinge, *Hip Replacement: The Facts*, Oxford University Press, 1983.
17. Y.H. An, Ed., *Orthopaedic Issues in Osteoporosis*, CRC Press, 2002.
18. D. Feldman. (2002, April). Orthopedics sector booming once as demand grows. *BBI*

Newsletter.[Online]Available:www.findarticles.com/cf_dls/m3570/4_25/84455336/pl
19. A. Kahn, *Arthritis*, Contemporary Books, Inc., 1983.
20. M.C. Hochberg, "Prevention of lower limb osteoarthritis: Data from the John Hopkins precursors study," in *The Many Faces of Osteoarthritis*, V.C. Hascall and K.E. Kuettner, Eds. Birkhauser Verlag, 2002, pp 31-37.
21. H.C. Amstutz and W.C. Kim, "Osteoarthritis of the hip," in *Osteoarthritis: Diagnosis and Management*, RW. Moskowitz, D.S. Howell, V.M Goldberg, and H.J. Mankin, Eds. W. B. Saunders Co., 1984, pp 442.
22. A.S. Hoffman, J.E. Lemons, F.J. Schoen, and B.D. Ratner, Eds., *Biomaterials Science: An Introduction to Materials in Medicine*, Academic Press: San Diego, 1996.
23. W.D. Callister, "*Materials Science and Engineering: An Introduction*," John Wiley & Sons, Inc., 1997.
24. K. Brummit and C.S. Hardaker, "Estimation of wear in total hip replacement using a ten station hip simulator," in *Advances in Medical Tribology: Orthopaedic implants and implant materials*, D. Dowson, Ed., MEP, 1998, pp 47-50.
25. G.W. Stachowiak, G.B. Stachowiak, and P. Campbell, "Application of numerical descriptors to the characterization of wear particles obtained form joint replacements," in *Advances in medical Tribolgy: Orthopaedic implants and implant materials*, D. Dowson, Ed., MEP, 1998, pp 93-102.
26. J. Larsen-Basse, "Introduction to Friction," in *ASM Handbook: Friction, Lubrication and Wear Technology*, S. Henry, Ed., ASM International, vol. 18, 1992, pp. 25-26.
27. D. Dowson, "Friction and wear of medical implants and prosthetic devices," in *ASM Handbook: Friction, Lubrication and Wear Technology*, S. Henry, Ed., ASM International, vol. 18, 1992, pp. 656-664.
28. S.N Gorb and M. Scherege, *Biological Micro- and Nanotribology*, Springer, 2001
29. H. Schmidt, A. Schminke, and D.M. Ruck, "Tribological behaviour of ion implanted Ti6Al4V sliding against polymers," *Wear*, vol. 209, pp. 49-56, 1997
30. P.J. Blau, Ed., "Glossary of Terms," in *ASM Handbook: Friction, Lubrication and Wear Technology*, S. Henry, Ed., ASM International, vol. 18, 1992, pp 1-21.
31. J.A. Tichy and D.M. Meyer, "Review of solid mechanics in tribology," *Int. J. of Solidz and Structures*, vol. 37, 2000, pp. 391-400.
32. J.H. Tylczak, "Abrasive wear," in *ASM Handbook: Friction, Lubrication and Wear Technology*, S. Henry, Ed., ASM International, vol. 18, 1992, pp. 185-190.
33. A.D. Sarkar, Friction and Wear, Academic Press, 1980.
34. B. Bhushan, *Introduction to Tribology*, John Wiley & Sons, 2002.
35. K.C. Ludema, "Sliding and Adhesive Wear," in *ASM Handbook: Friction, Lubrication and Wear Technology*, S. Henry, Ed., ASM International, vol. 18, 1992, pp. 236-241.
36. B.W. Madsen, "Corrosive Wear," in *ASM Handbook: Friction, Lubrication and Wear Technology*, S. Henry, Ed., ASM International, vol. 18, 1992, pp. 271-279.
37. A.W. Ruff, "Wear Measurement," in *ASM Handbook: Friction, Lubrication and Wear Technology*, S. Henry, Ed., ASM International, vol. 18, 1992, pp. 362-369.

38. F.M. Kustas and M.S. Misra, "Friction and Wear of Titanium Alloys," in *ASM Handbook: Friction, Lubrication and Wear Technology*, S. Henry, Ed., ASM International, vol. 18, 1992, pp. 778-794.
39. R. Hubler, "Hardness and corrosion protection enhancement behaviour of surgical implant surfaces treated with ceramic thin films," *Surface & Coatings Tech.*, vol. 116-119, 1999, pp. 1111-1115.
40. Y. Fu and H. Du, "Effects of the counterface materials on the tribological characteristics of CN_X coating deposited on plasma-nitrided Ti-6Al-4V," *Mater. Sci. & Eng. A.*, vol. 298, 2001, pp. 16-25.
41. M. Long and H.J. Rack, "Friction and surface behavior of selected titanium alloys during reciprocating-sliding motion," *Wear*, vol. 249, 2001, pp. 158-168.
42. P.A. Dearnley, K.L. Dahm, and H. Cimenoglu, "The corrosion-wear behaviour of thermally oxidized CP-Ti and Ti-6Al-4V," *Wear*, (article in press)
43. R.F. Bunshah, "PVD and CVD Coatings," in *ASM Handbook: Friction, Lubrication and Wear Technology*, S. Henry, Ed., ASM International, vol. 18, 1992, pp. 840-849.
44. M. Long and H.J Rack, "Titanium alloys in total joint replacement-a materials science perspective," *Biomaterials*, vol. 19, 1998, pp. 1621-1639.
45. R.A. Buchanan, R.K. Bacon, J.M. Williams, and G.M. Beardsley, "Ion Implantation to improve the corrosive-wear resistance of surgical Ti-6Al-4V, "Transactions: Society for Biomaterials, Vol. VI, 106 , 1983.
46. J.M. Williams, R.A. Buchanan, "Effects of N-Implantation on the corrosive-wear properties of surgical Ti-6Al-4v alloy," Ion Implantation and Ion Beam Processing of Materials, G.K. Hubler, O.W. Holland, C.R.Clayton, and C.W. White, Eds., Elsevier, New York, pp.735-740, 1984.
47. E.D. Rigney, Jr., R.A. Buchanan, and J.M. Williams, "Effects of nitrogen and carbon ion implantation on the corrosive wear behavior of Ti-6Al-4V in serum solutions," Seventeenth International Biomaterials Symposium, San Diego, California, Transactions: Society for biomaterials, Vol. VII, 1985.
48. J.M. Williams and R.A. Buchanan, "Ion implantation of surgical Ti-6Al-4V alloy," Mater. Sci. Engr., Vol. 69, 1985, pp. 237-246.
49. R.A. Buchanan, E.D. Rigney, Jr., and J.M. Williams, "Influence of stress on the wear-accelerated corrosion of nitrogen ion implanted Ti-6Al-4V, "Eighteenth International Biomaterials Symposium, Minneapolis, Minnesota, Transactions: Society for biomaterials, Vol. IX, 34, 1986.
50. J. M. Williams, R.A. Buchanan, and E.D. Rigney, Jr., "Improvement in wear performance of surgical Ti-6Al-4V alloy by ion implantation of nitrogen and carbon," Ion Plating and Implantation: Application to Materials, Metals/Materials Technology Series 8504-008, American Society for Metals, Metals Park, Ohio, pp. 1-10, 1986.
51. R.A. Buchanan, E.D. rigney, Jr., and J.M. Williams, "Ion implantation of surgical Ti-6Al-4V for improved resistance to wear accelerated corrosion," Journal of Biomedical Materials Research, Vol. 21, No. 3, 1987, pp. 355-366.
52. R.A. Buchanan, E.D. Rigney, Jr., and J.M. Williams, "Wear-accelerated corrosion of Ti-6Al-4V and nitrogen ion-implanted Ti-6Al-4V: mechanisms and influence

of fixed-stress magnitude," Journal of Biomedical Materials Research, Vol. 21, No. 3, 1987, pp. 367-377.
53. G.R. Fenske, "Ion Implantation," in *ASM Handbook: Friction, Lubrication and Wear Technology*, S. Henry, Ed., ASM International, vol. 18, 1992, pp. 850-860.
54. F. Torregrosa, L. Barrallier, and L. Roux, "Phase analysis, microhardness and tribological behaviour of Ti-6Al-4V after ion implantation of nitrogen in connection with its application for hip-joint prosthesis," *Thin Solid Films*, vol. 266, 1995, pp. 245-253.
55. Y. Itoh, A. Itoh, H. Azuma, and T. Hioki, "Improving the tribological properties of Ti-6Al-4V alloy by nitrogen-ion implantation," *Surf. Coat Technol*, vol. 111, 1999, pp. 172-176.
56. C.A. Stickels, "Carburizing," in *ASM Handbook: Friction, Lubrication and Wear Technology*, S. Henry, Ed., ASM International, vol. 18, 1992, pp. 873-877.
57. F.T. Hoffmann and P. Mayr, "Nitriding and Nitrocarburizing," in *ASM Handbook: Friction, Lubrication and Wear Technology*, S. Henry, Ed., ASM International, vol. 18, 1992, pp. 878-883.
58. B.S. Yilbas, A.Z. Sahin, A.Z. Garni, S.A.M Said, Z. Ahmed, B.J. Abdulaleem, and M. Sami, "Plasma nitriding of Ti-6Al-4V to improve some tribological properties," Surf. Coat. Technol., vol. 80, 1996, pp. 287-292.
59. D. Rodriguez, F.J. Gil, and J.A. Planell, "Wear resistance of the nitrogen diffusion hardening of the Ti-6Al-4V alloy," in proceeding from 11th Conference of ESB in Toulouse France, 1998.
60. M.A. Khan, R.L. Williams, and D.F. Williams, "In-vitro corrosion and wear of titanium alloys in the biological environment," *Biomaterials*, vol. 17, 1996, pp. 2117-2126.
61. W. F. Ho, C.P. Ju, and J.H. Chern Lin, "Structure and properties of cast binary Ti-Mo alloys," *Biomaterials*, vol. 20, 1999, pp. 2115-2122.
62. D.J. Lin, J.H. Chern Lin, and C.P. Ju, "Structure and properties of Ti-7.5Mo-xFe alloys," Biomaterials, vol. 23, 2003, pp. 1723-1730.
63. M. Niinomi, D. Kuroda, K. Fukunaga, M. Morinaga, Y. Kato, T. Yashiro, and A. Suzuki, " Corrosion wear fracture of new β type biomedical titanium alloys," Mater. Sci. Eng. Vol. A263, 1999, pp. 193-199.
64. M.A. Khan, R.L. Williams, and D.F. Williams, "Conjoint corrosion and wear in titanium alloys," *Biomaterials*, vol. 20, 1999, pp. 765-772.
65. E.E. Stansbury and R.A. Buchanan, *Fundamentals of Electrochemical Corrosion*, ASM International, 2000.
66. M.A. Khan, R.L. Williams, and D.F. Williams, "The corrosion behaviour of Ti-6Al-4V, Ti-6Al-7Nb, and Ti-13Nb-13Zr in protein solutions," *Biomaterials*, vol. 20, 1999, pp. 631-637.
67. M.F. Lopez, A. Gutierrez, J.A. Jimenez, "In vitro corrosion behaviour of titanium alloys without vanadium," *Electrochimica Acta*, vol. 47, 2002, pp. 1359-1364.
68. M.L. Escudero, M.F. Lopez, J. Ruiz, M.C. Garcia-Alonso, H. Canahua, *J. Biomed. Mater. Res.*, vol. 31, 1996, pp. 313.

69. C. Kuphasuk, Y. Oshida, C.J Andres, S.T. Hovijitra, M.T. Barco, and D.T. Brown, "Electrochemical corrosion of titanium and titanium-based alloys," *J Prosth Dent*, vol. 85(2), 2001, pp. 195-202.
70. M. Aziz-Kerrzo, K.G. Conroy, A.M. Fenelon, S.T. Farrel, and C.B. Breslin, "Electrochemical studies on the stability and corrosion resistance of titanium–based implant materials," *Biomaterials*, vol. 22, 2001, pp. 1531-1539.
71. Y. Okazaki, S. Rao, Y. Ito, and T. Tateishi, "Corrosion resistance, mechanical properties, corrosion fatigue strength and cytocompatibility of new Ti alloys without Al and V," *Biomaterials*, vol. 19, 1998, 1197-1215.
72. I.C. Clarke, "Wear of artificial joint materials I, Friction and wear studies: Validity of wear-screening protocols." *Engr Med*, Vol 10 (3), 1981, pp 115-122.
73. C. Abreu, M. Amarai, F.J. Oliveira, J.D. Santos, R.F. Silva, and J.R. Gomes. "Tribological characterization of Si_3N_4 bioglass biocomposite in self-mating experiments and dissimilar tests against UHMWPE," Key Engineering Materials, Vols. 230-232, 2002, pp. 487-490.
74. S. Hiromoto, A.P. Tsai, M. Sumita, and T. Hanawa. "Effect of surface finish and dissolved oxygen on the polarization behavior of the Zr-65Al-7.7Ni-10Cu17.5 amorphous alloys in phosphate buffered solution" Corr Sci, Vol. 42, 2000, pp. 2167 – 2185.

APPENDICES

APPENDIX OF TABLES

Table 1. Cytoxicity ranking of various metal ions. Evaluated in L-929 or 3T3 Mouse Fibroblast Cultures.

Watteha et al., 1991[b]	Watteha et al., 1994[ab]	Schmatz et al., 1997[ba]	Sauvant et al., 1997[a]	Yamamoto et al., 1998[a]		Kappert et al., 1998[a]
Cd^{2+}	Cd^{2+}	Ag^{+}	Cu^{2+}, V^{5+}	Cd^{2+} (most toxic)	Y^{3+}	In^{3+}
Ag^{+}	Ag^{+}	**Zn^{2+}**	Hg^{2+}, Zn^{2+}	V^{3+}	W^{6+}	Ga^{3+}
Zn^{2+}	**Zn^{2+}**	Cd^{2+}	Co^{2+}	Ag^{+}	Fe^{3+}	**Zn^{2+}**
Cu^{2+}	V^{3+}	Hg^{2+}	Cd^{2+}	Hg^{2+}	Pd^{2+}	Cu^{2+}
Ga^{3+}	Au^{3+}	Au^{3+}	Ti^{4+}	Pb^{2+}	Fe^{2+}	Au^{3+}
Au^{4+}	Cu^{2+}	Pt^{4+}	Nb^{5+}	Be^{2+}	Ti^{4+}	Co^{2+}
Ni^{2+}	Co^{2+}	Co^{2+}	Fe^{3+}	In^{3+}	Hf^{4+}	Ni^{2+}
Pd^{2+}	Pd^{2+}	Cu^{2+}	Sb^{3+}	Cr^{3+}	Ru^{3+}	Pd^{2+}
In^{3+}	Ti^{4+}	Ni^{2+}	Sn^{4+}	Hg^{+}	Sr^{2+}	Sn^{2+}
	Be^{2+}	Pd^{2+}	Mn^{3+}, Ge^{4+}	Cu^{2+}	Sn^{4+}	Mo^{5+}
	Ga^{3+}	Mn^{2+}	Cr^{3+}	Rh^{3+}	Ba^{2+}	La^{3+}
	Ni^{2+}	Nb^{5+}	Pb^{2+}	Ti^{3+}	Cs^{+}	
	Ti^{4+}	Ga^{3+}	Ba^{2+}	Sn^{2+}	Nb^{5+}	
	Cr^{3+}	Cr^{3+}		Ga^{3+}	Ta^{5+}	
	Al^{3+}	In^{3+}		Pb^{2+}	Zr4+	
		Sn^{2+}		Cu^{+}	Al^{3+}	
				Mn^{2+}	Mo^{5+}	
				Ti^{+}	Rb^{+}	
				Ni^{2+}	Li^{+} (least toxic)	
				Zn^{2+}		

Bold-face elements were investigated in all studies. Table adapted from reference 14.

Table 2. Composition of the phosphate buffered saline (PBS) solution.

Composition	NaCl	Na_2HPO_4	KCl	KH_2PO_4
Concentration (10^{-3} x M)	137	8.12	2.68	1.47

Table 3. Average mass loss values of Ti-6Al-4V and Ti-8Mo.

Titanium Alloy	ML_{corr} (g)	ML_{wear} (g)
Ti-6Al-4V	3.26E-06	1.62E-03
Ti-8Mo	1.30E-05	1.43E-04

Table 4. Results of cyclic-anodic-polarization tests.

Titanium alloy	Test #	i_{corr} (mA/m^2)	Average i_{corr}	CPR (μm/y)	Average CPR (μm/y)
Ti-6Al-4V	1	0.54	0.39 ± 0.12	0.47	0.34 ± 0.11
	2	0.43		0.37	
	3	0.25		0.22	
	4	0.33		0.29	
Ti-8Mo	1	0.50	1.30 ± 0.80	0.42	1.10 ± 0.68
	2	2.07		1.77	
	3	1.88		1.61	
	4	0.71		0.61	

APPENDIX OF FIGURES

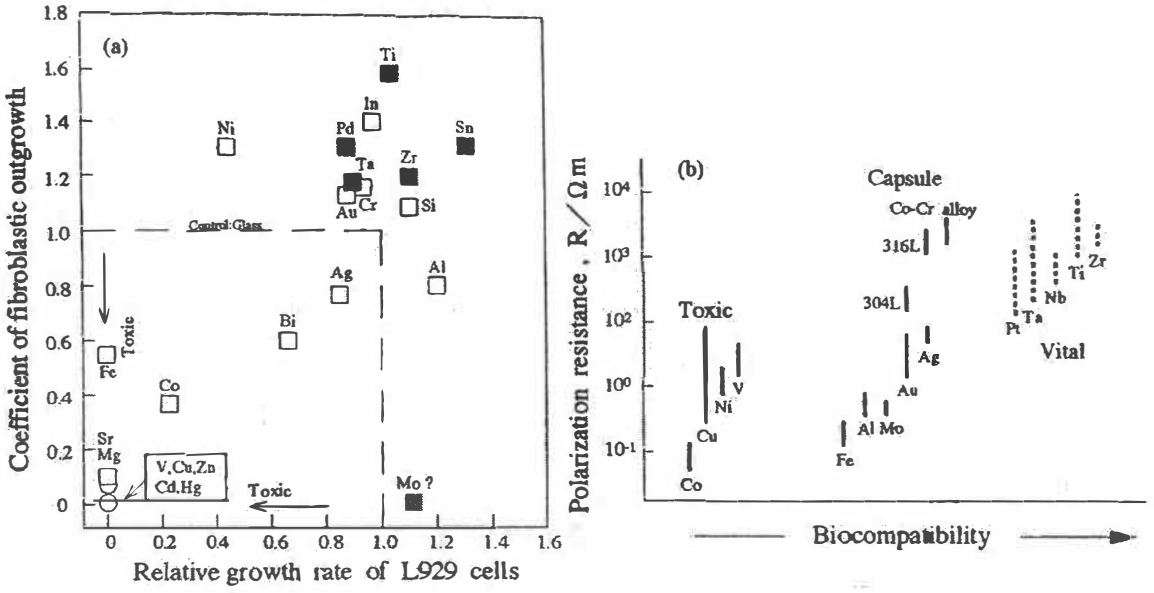

Figure 1. Biological safety of metals. Figure 1a shows the cytotoxicity of pure metals. Figure 1b shows the relationship between polarization resistance and biocompatibility of pure metals. From reference 11.

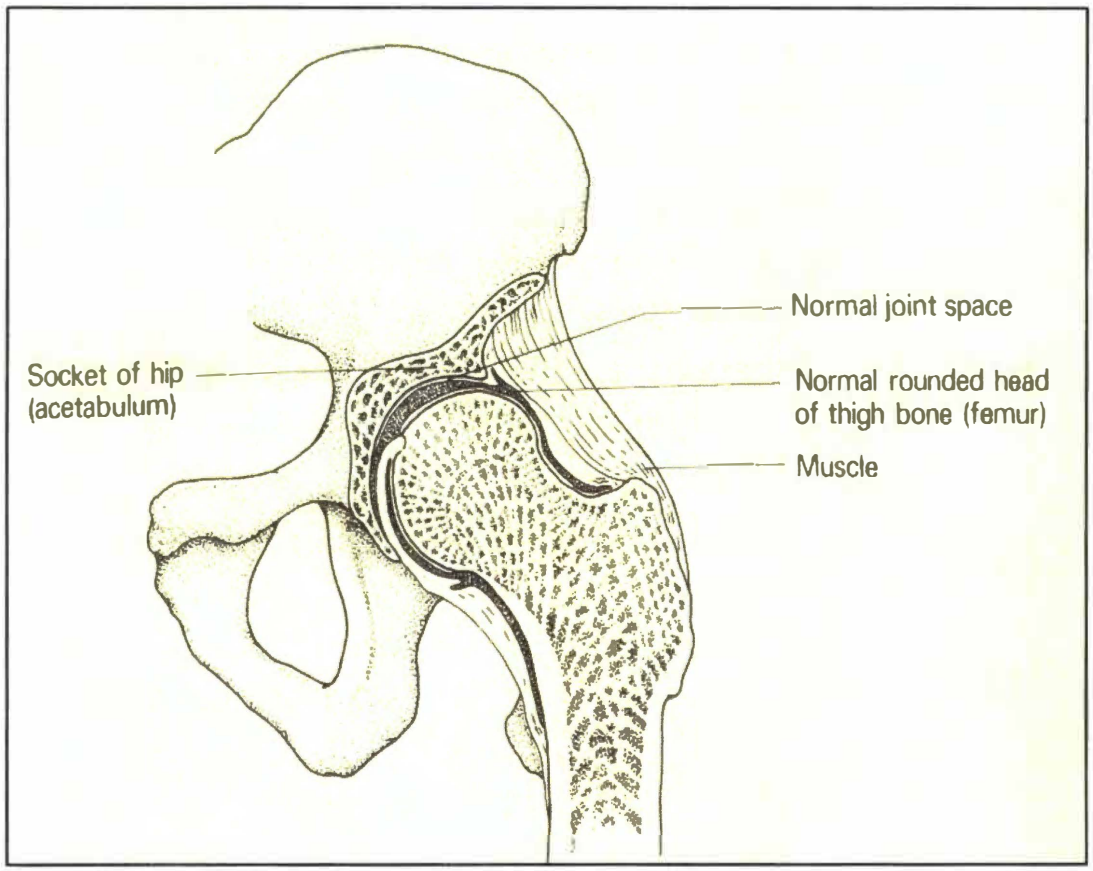

Figure 2. Illustration of a normal hip joint. (From reference 16)

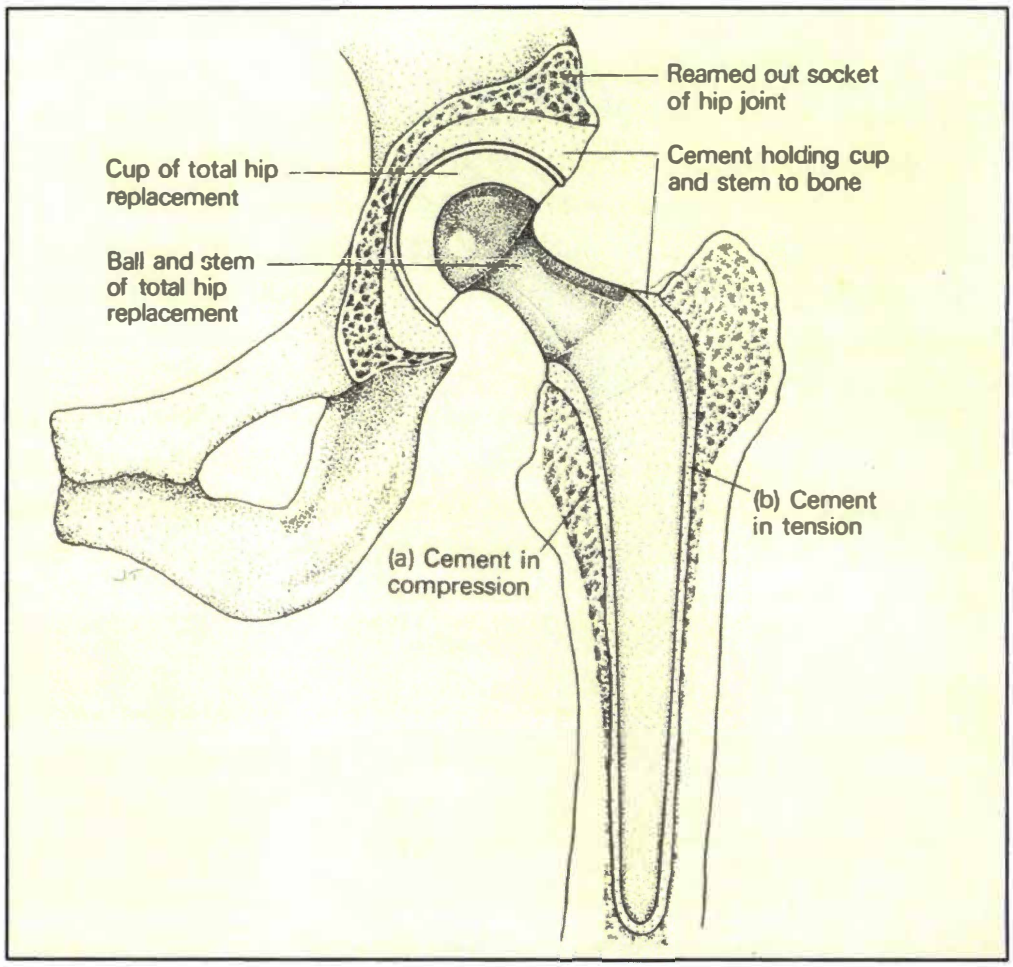

Figure 3. Illustration of a Charnley hip implant. (Adapted from reference 164)

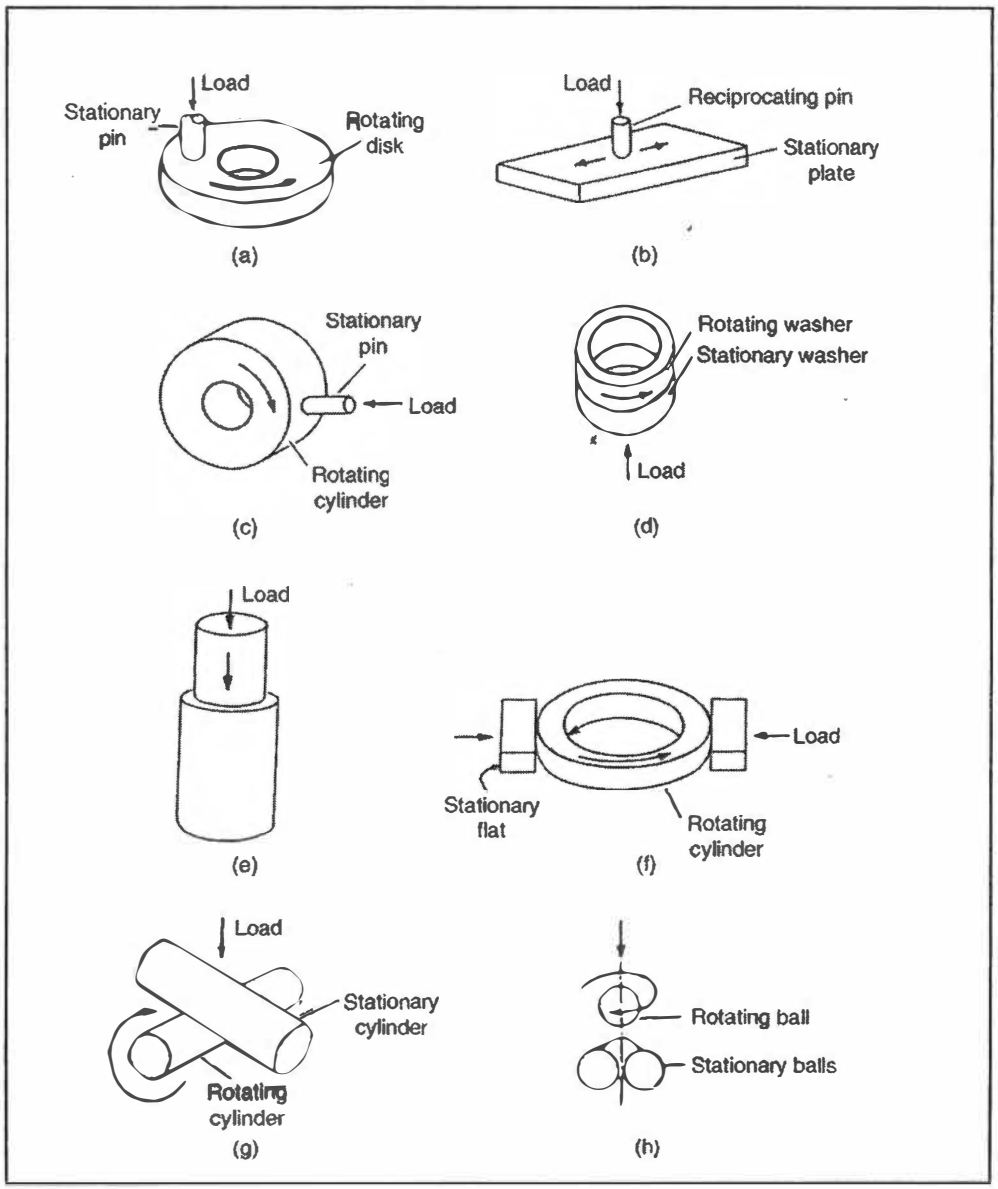

Figure 4. Various wear screening test geometries. (a) pin-on-disk, (b) pin-on-flat, (c) pin-on-cylinder, (d) thrust washers, (e) pin-into-brushing, (f) rectangular flats on rotating cylinder, (g) crossed cylinders, and (h) four ball. (Adapted from reference 34).

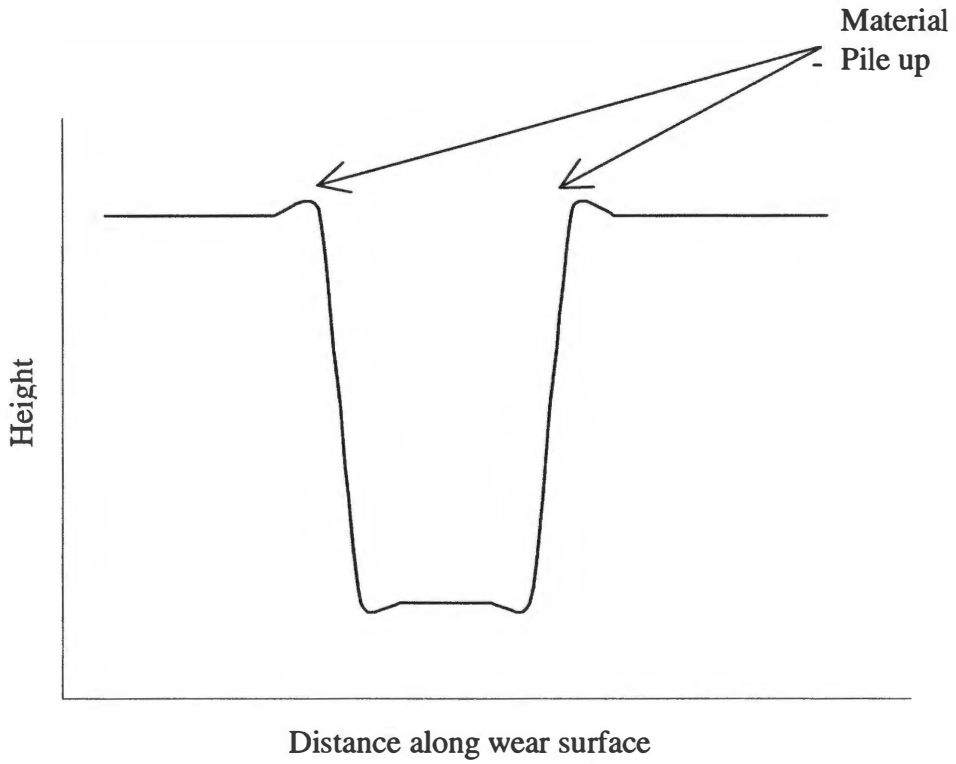

Figure 5. Example wear surface profile. Schematic is perpendicular to the sliding direction of the pin. Regions denoted as pile up represent displaced material due to plastic deformation.

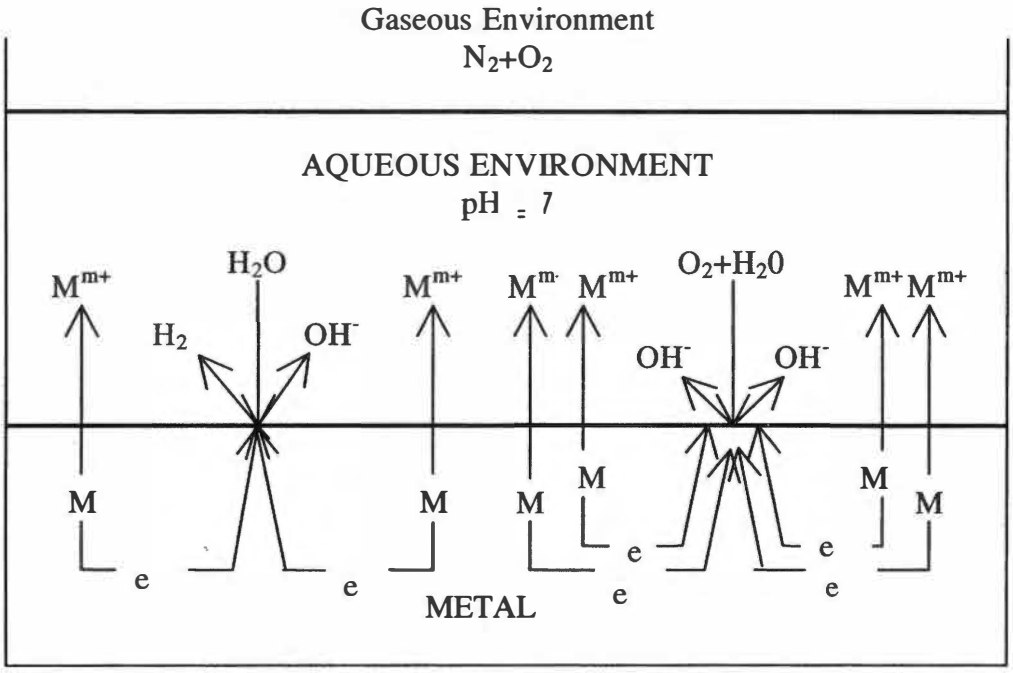

Figure 6. Uniform corrosion supported by the reduction of dissolved oxygen. (Adapted from reference 65)

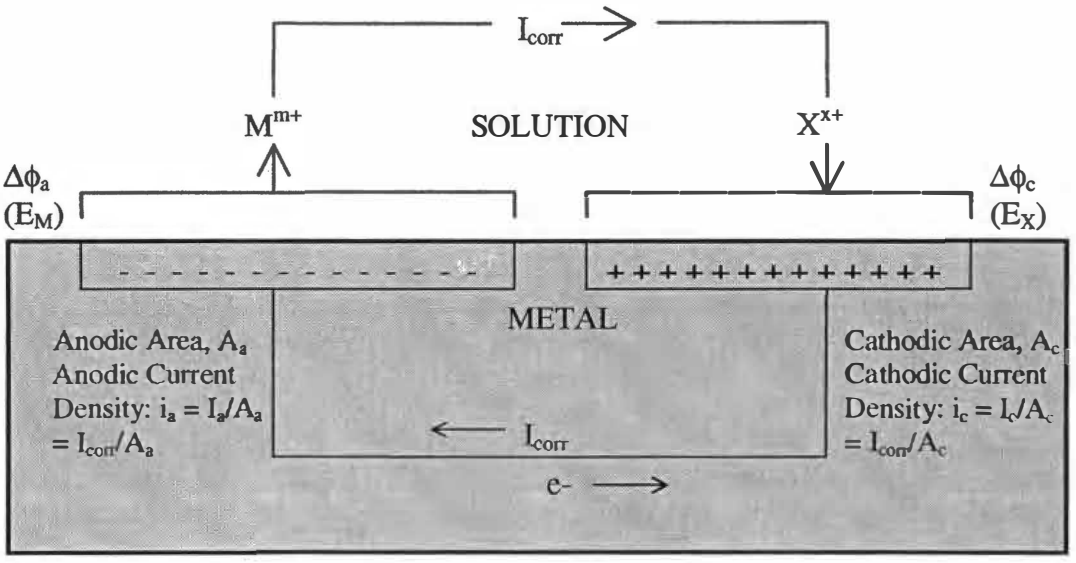

Figure 7. The electrochemical corrosion circuit. This figure shows relationships between anodic and cathodic areas, current densities, and potentials. (Adapted from reference 65)

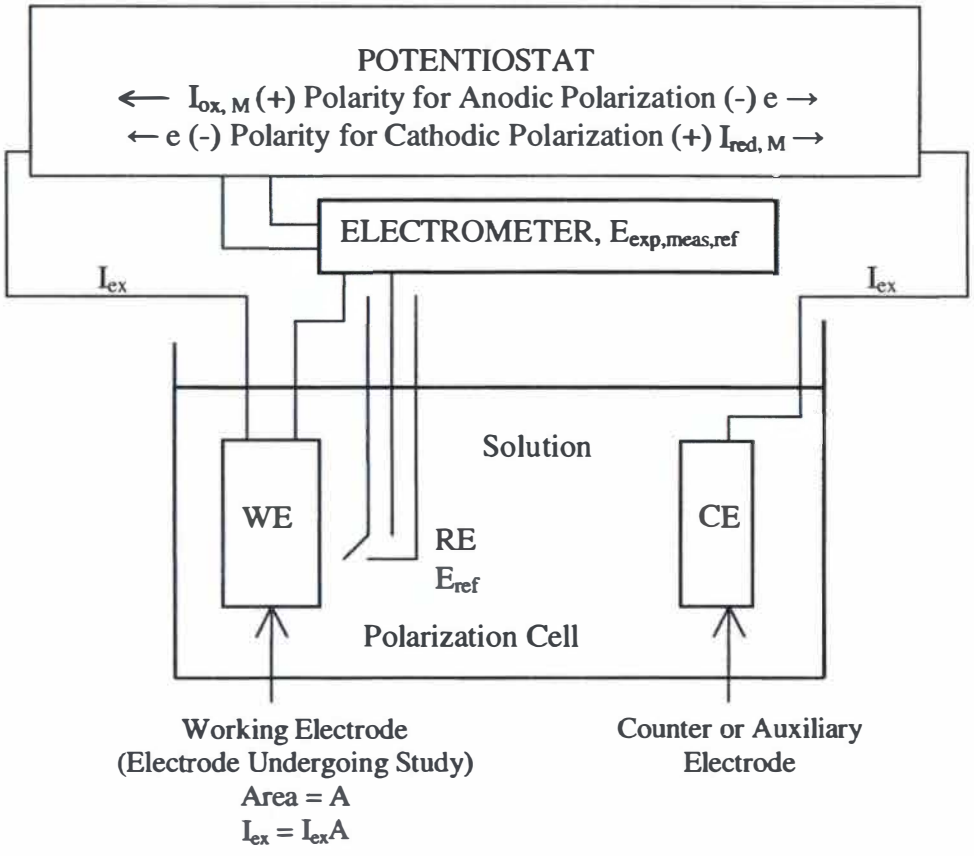

Figure 8. The potentiostatic circuit. (Adapted from reference 65)

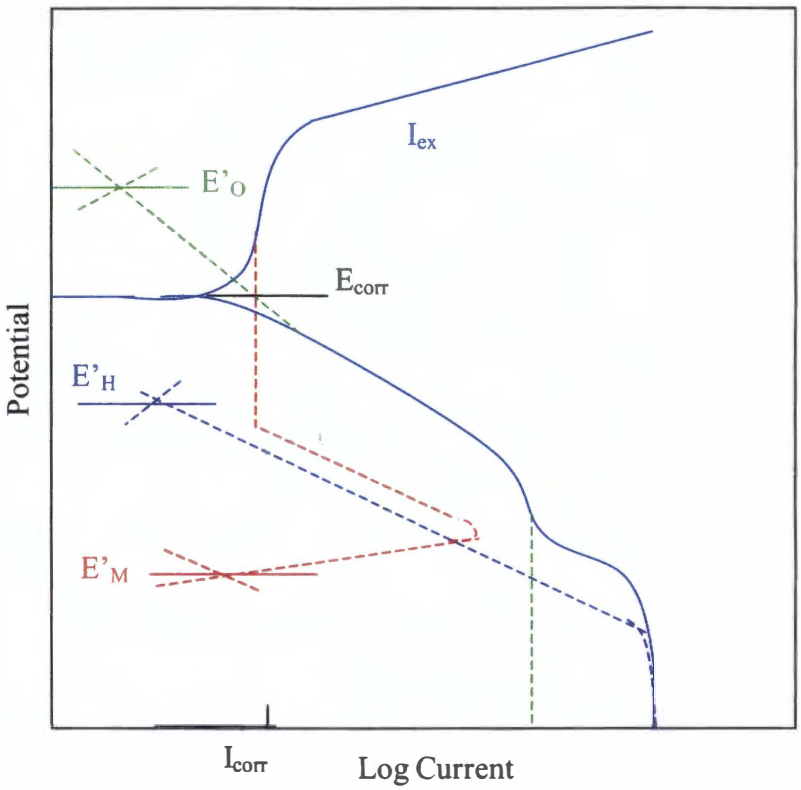

Figure 9. Schematic experimental polarization curves. Schematic of experimental curves (solid blue curves) assuming active-passive behavior for the individual metal-oxidation curve (dashed red) and Tafel behavior plus limiting diffusion for the individual dissolved oxygen (dashed green) and hydrogen-ion reduction curves (dashed dark blue). Note that the red, dark blue, and green curves represent equations 6, 7, 8, respectively. (Adapted from reference 65).

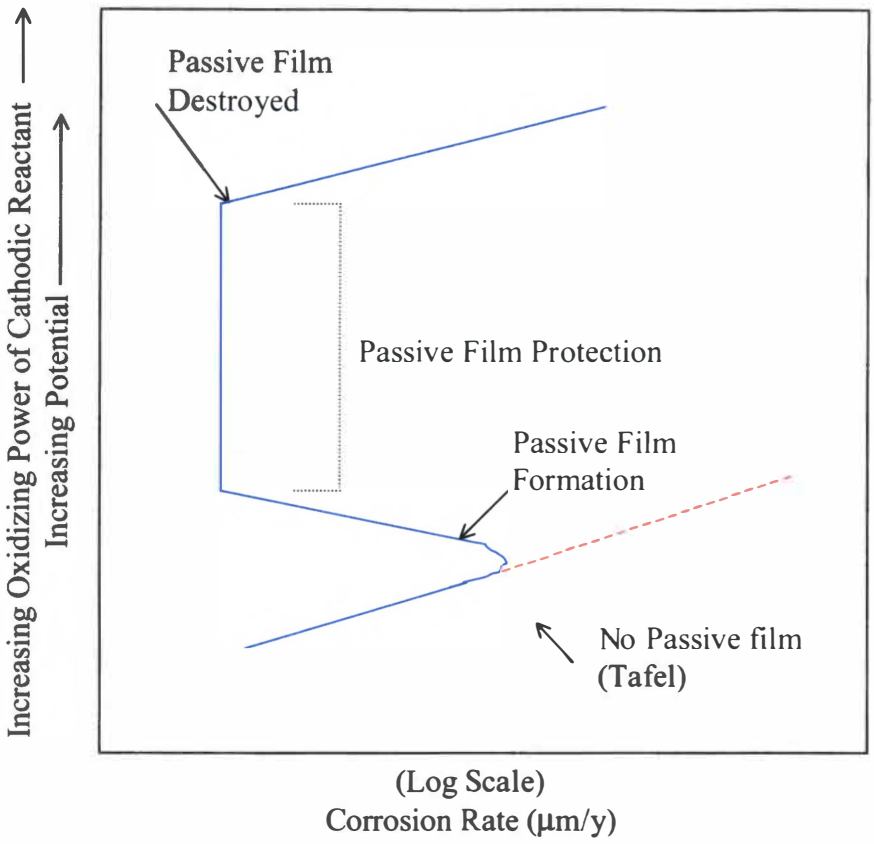

Figure 10. Active passive behavior compared with Tafel behavior. A Schematic comparison of the effect of increasing oxidizing power of the environment on the corrosion of an active passive alloy versus a Tafel alloy. (Adapted from reference 65)

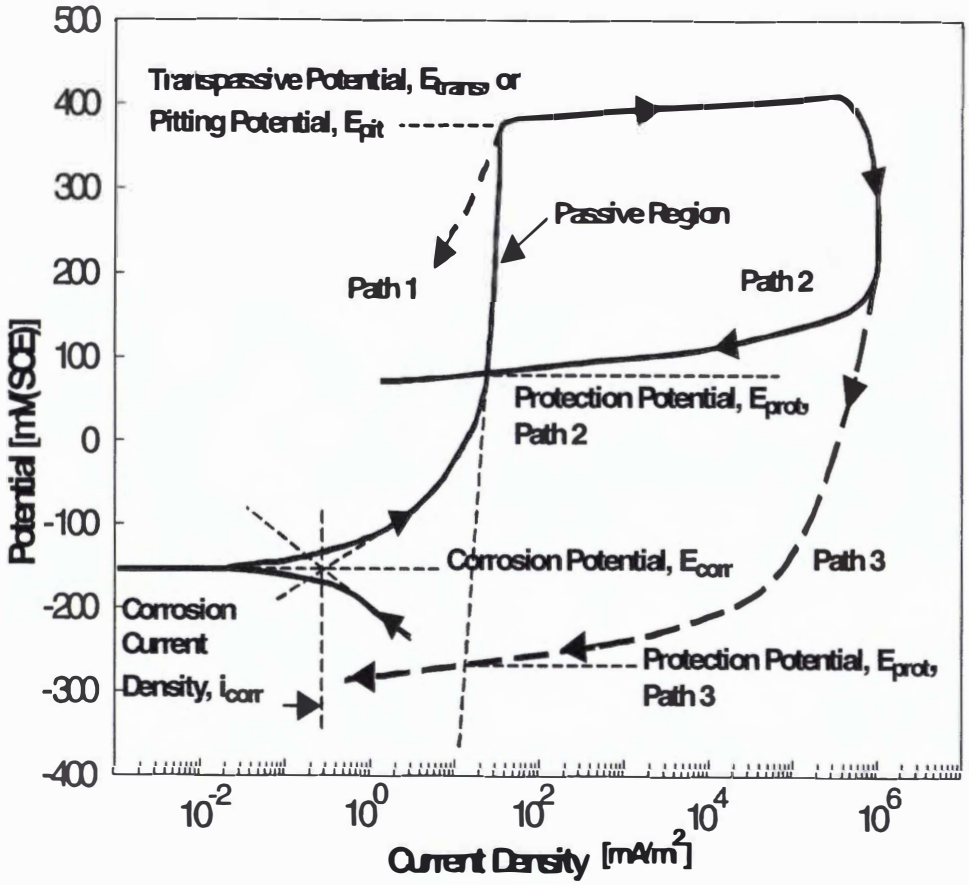

Figure 11. Schematic of possible paths during cyclic-anodic-polarization tests.

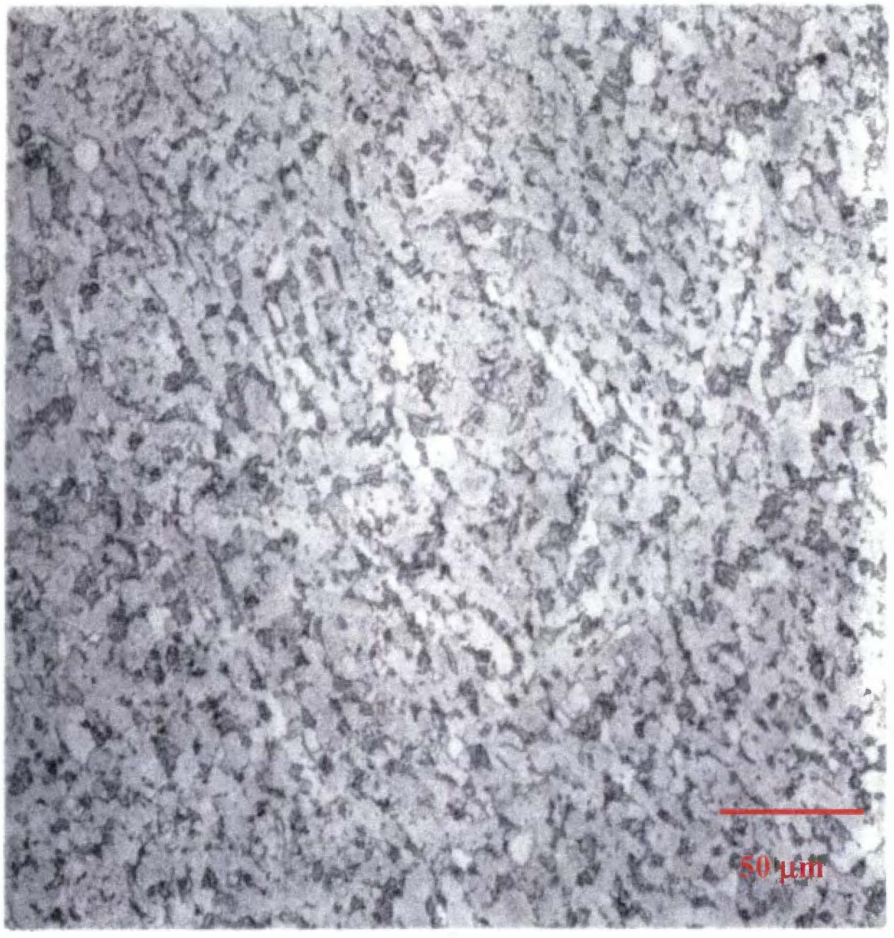

Figure 12. Micrograph of Ti-6Al-4V. The micrograph illustrates the duplex α (light regions) + β (dark regions) microstructure of Ti-6Al-4V.

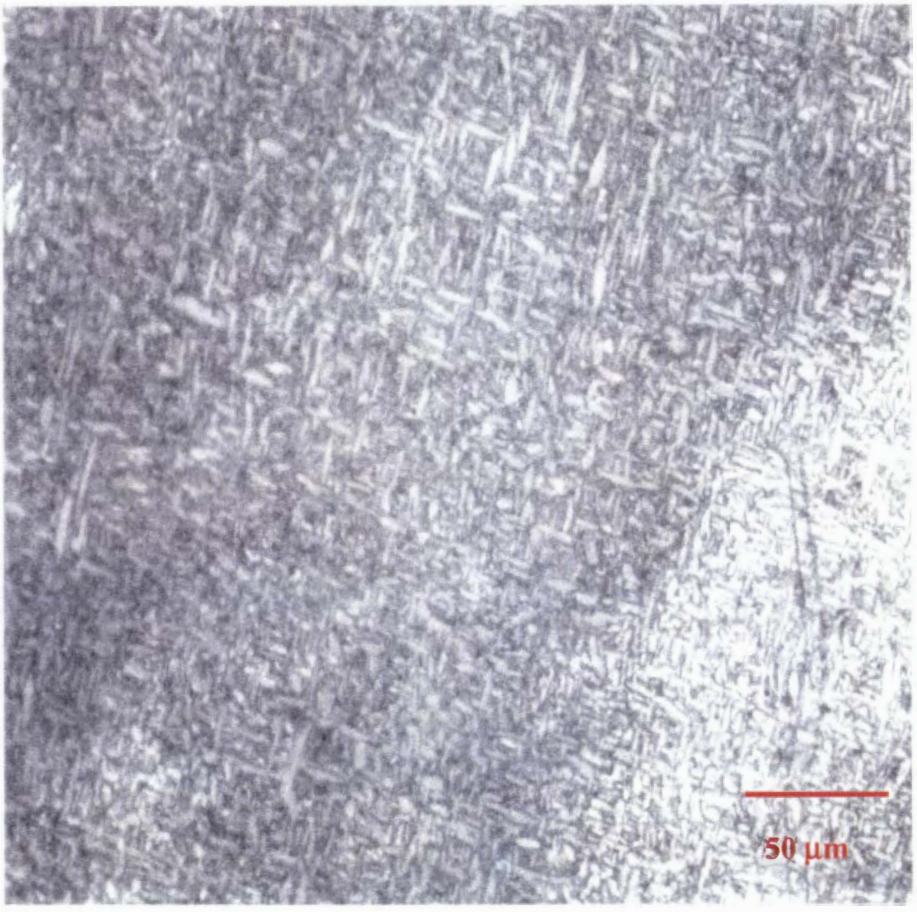

Figure 13. Micrograph of Ti-8Mo. The micrograph shows ω in a α + β structure.

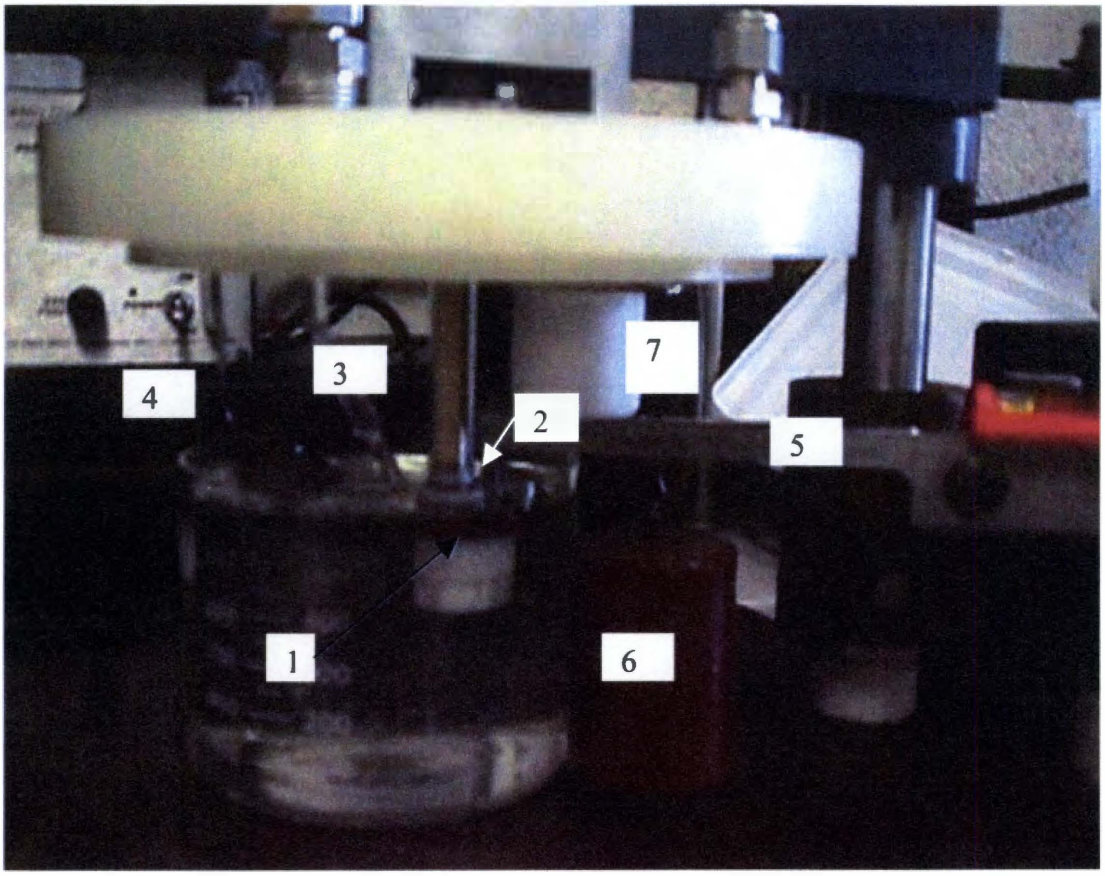

Figure 14. Wear experimental set-up. (1) disk sample (2) titanium bit (3) SCE (4) CE (5) wear arm (6) lead weight (7) cup closest to the pin

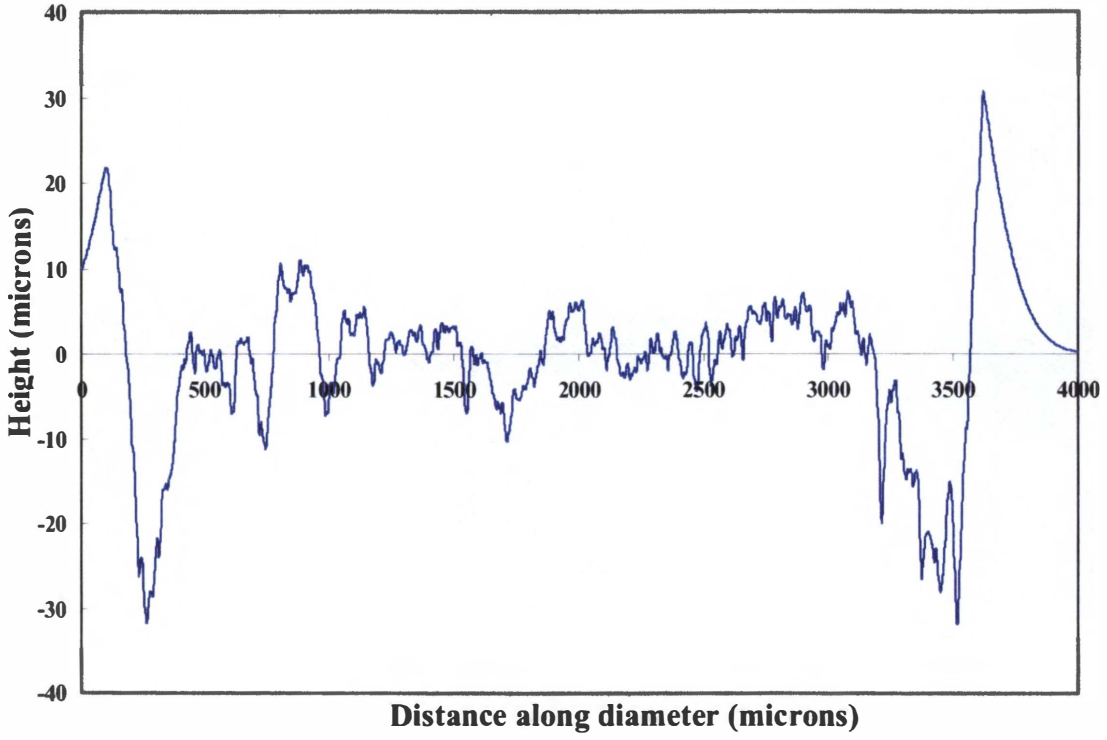

Figure 15. Profilometry scan of Ti-6Al4V.

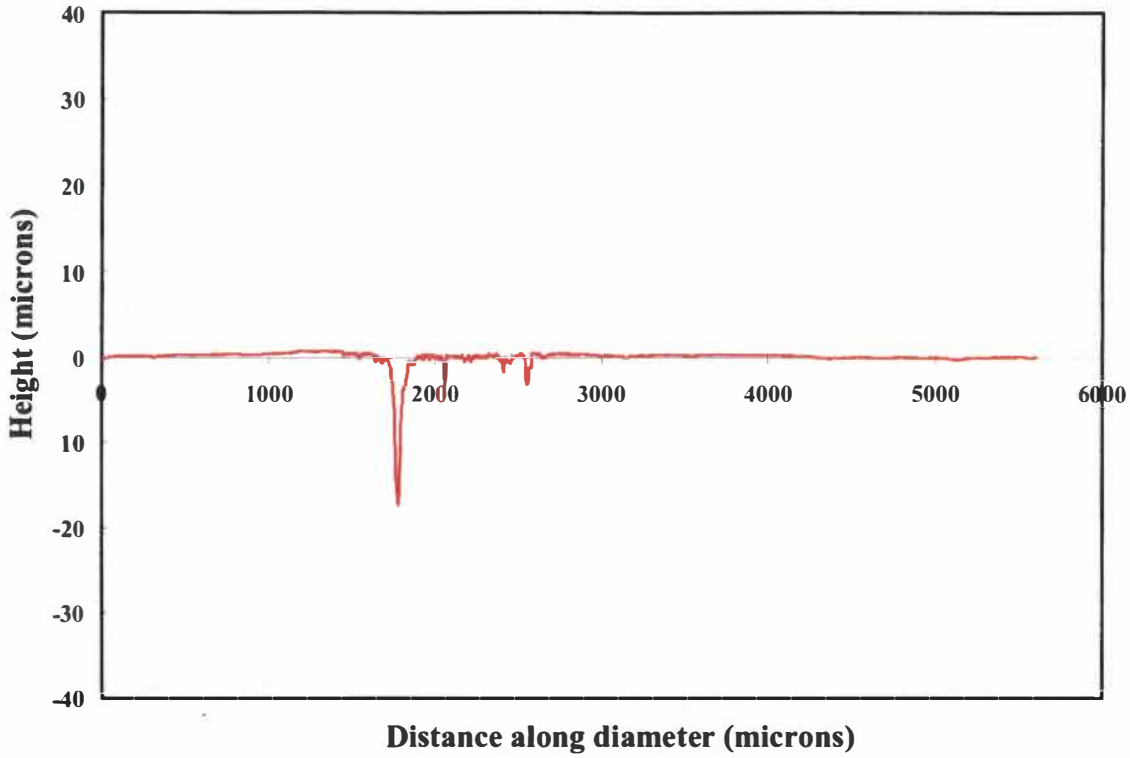

Figure 16. Profilometry scan of Ti-8Mo.

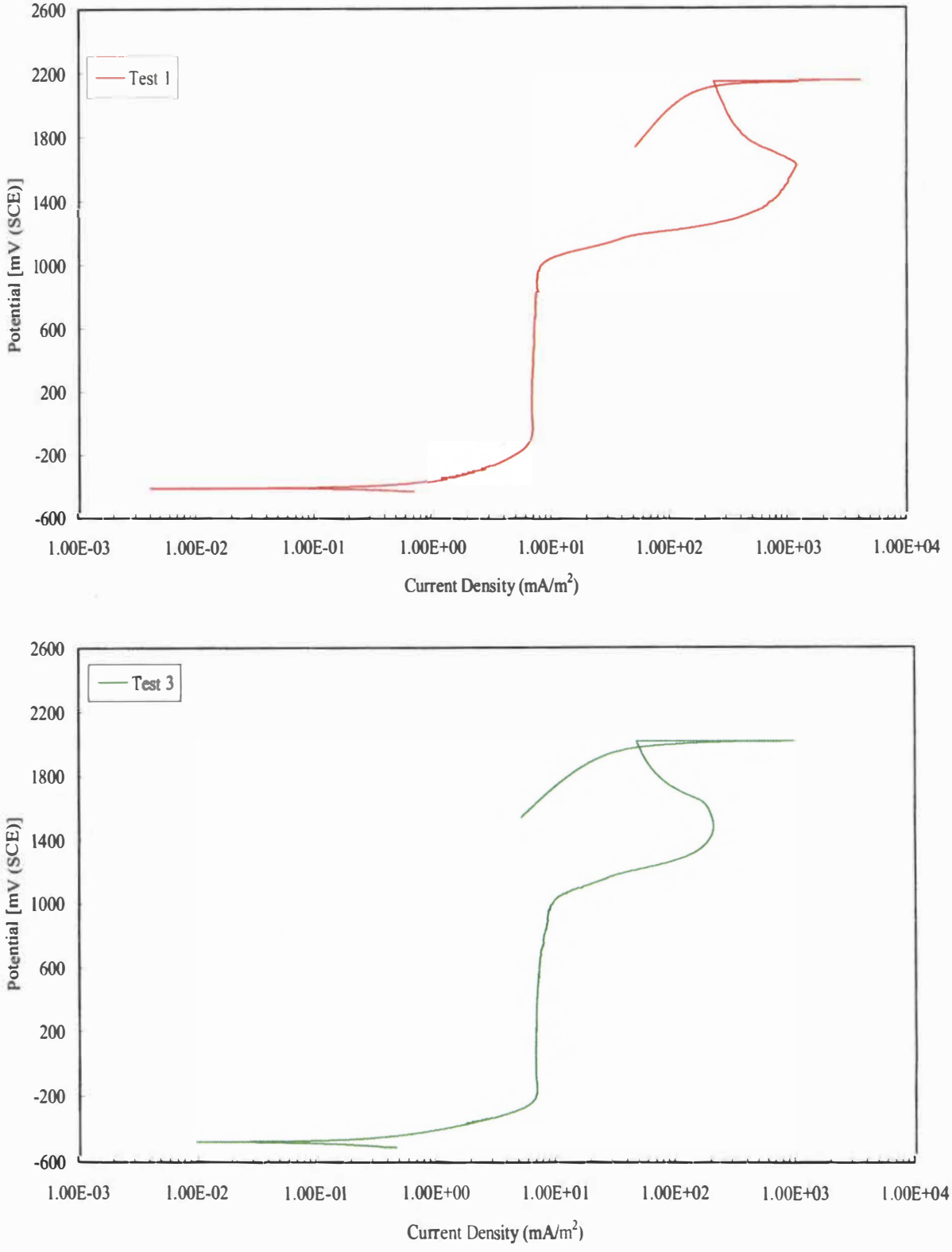

Figure 17. Cyclic-anodic-polarization curves of Ti-6Al-4V.

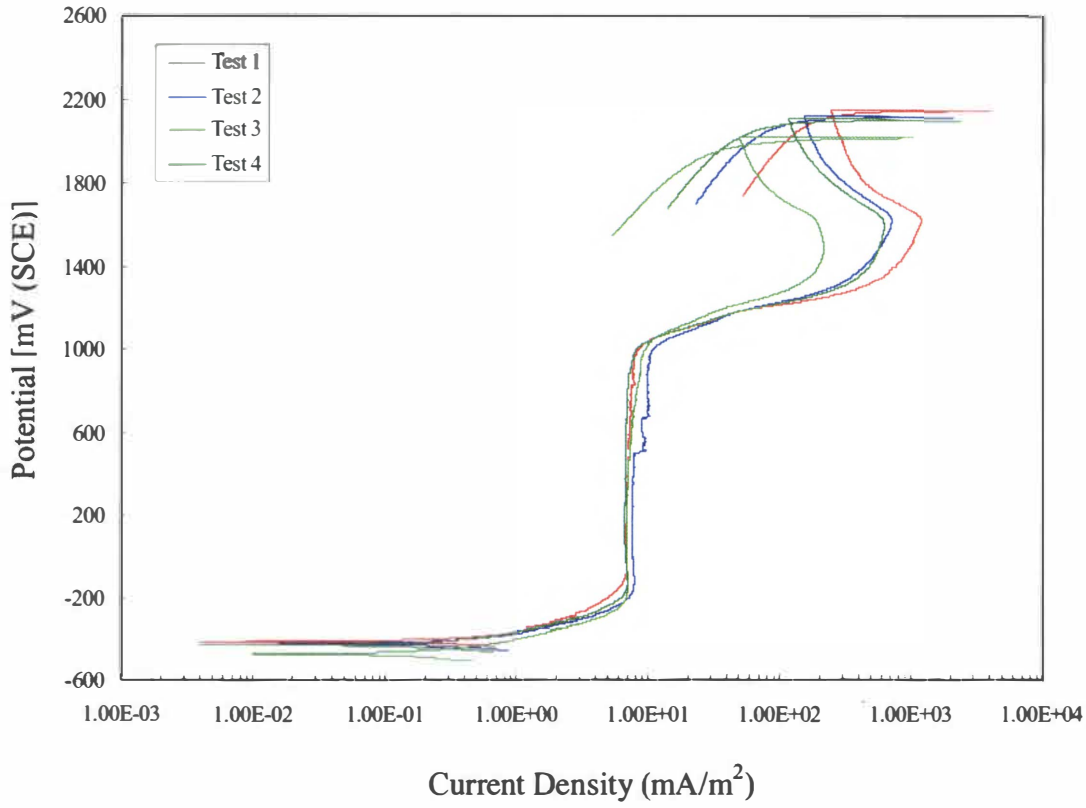

Figure 18. All cyclic-anodic-polarization scans of Ti-6Al-4V.

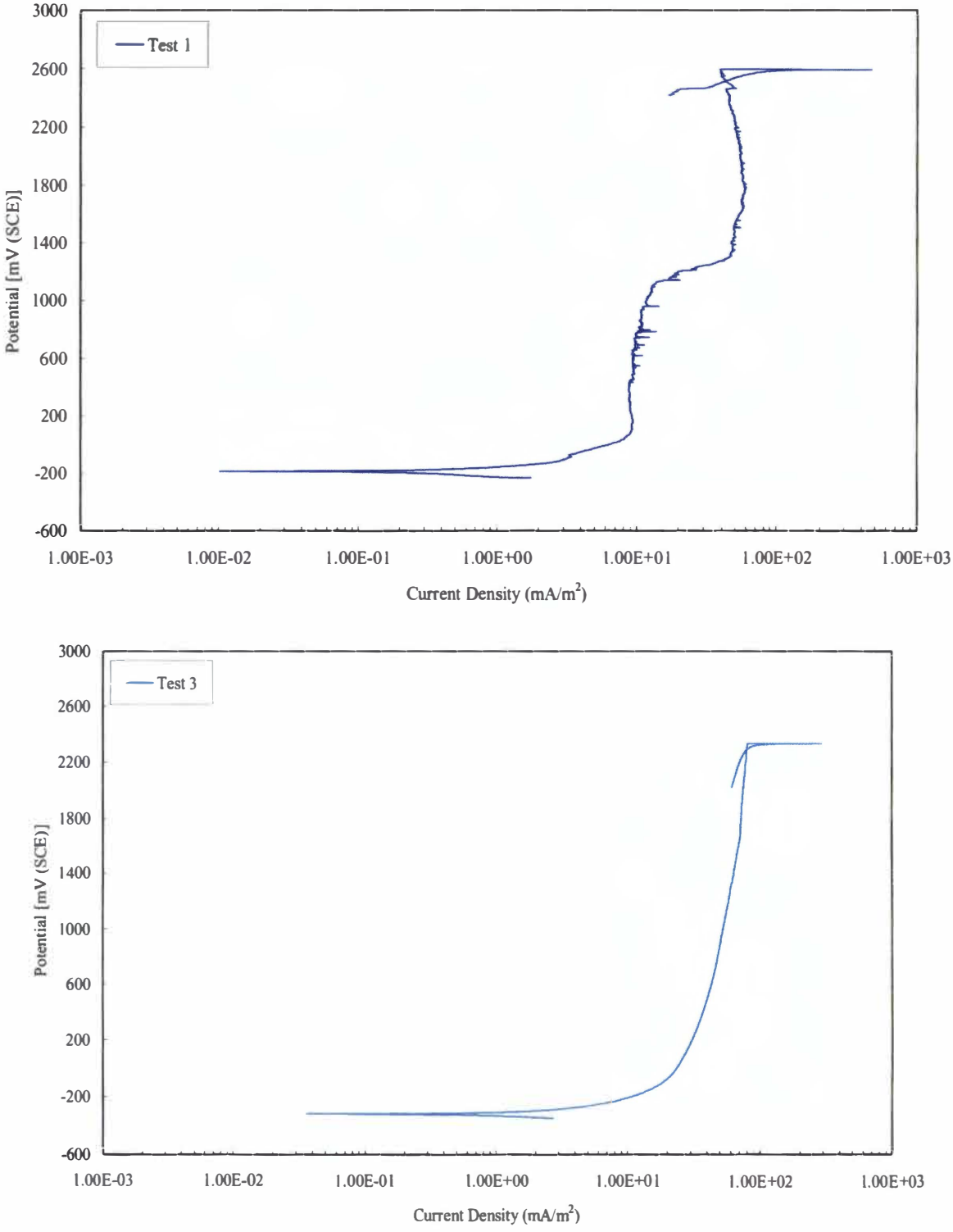

Figure 19. Cyclic-anodic-polarization curves for Ti-8Mo.

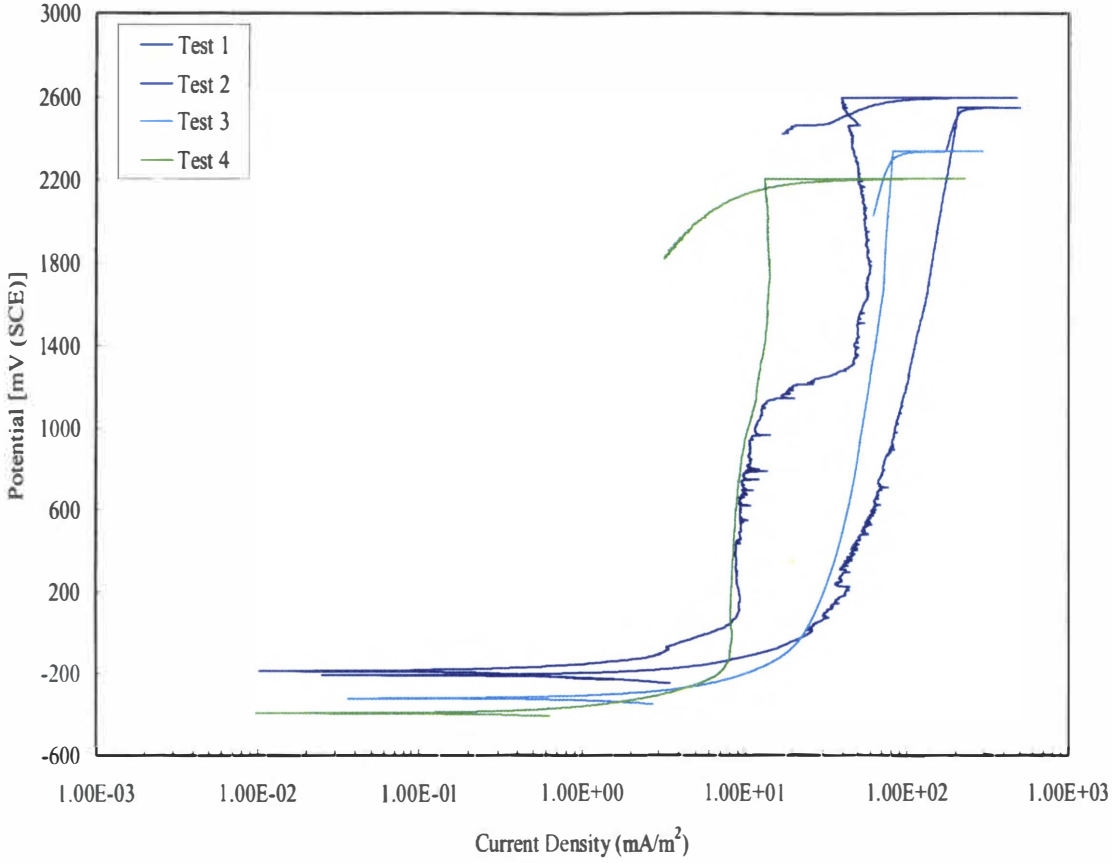

Figure 20. All cyclic-anodic-polarization scans of Ti-8Mo.

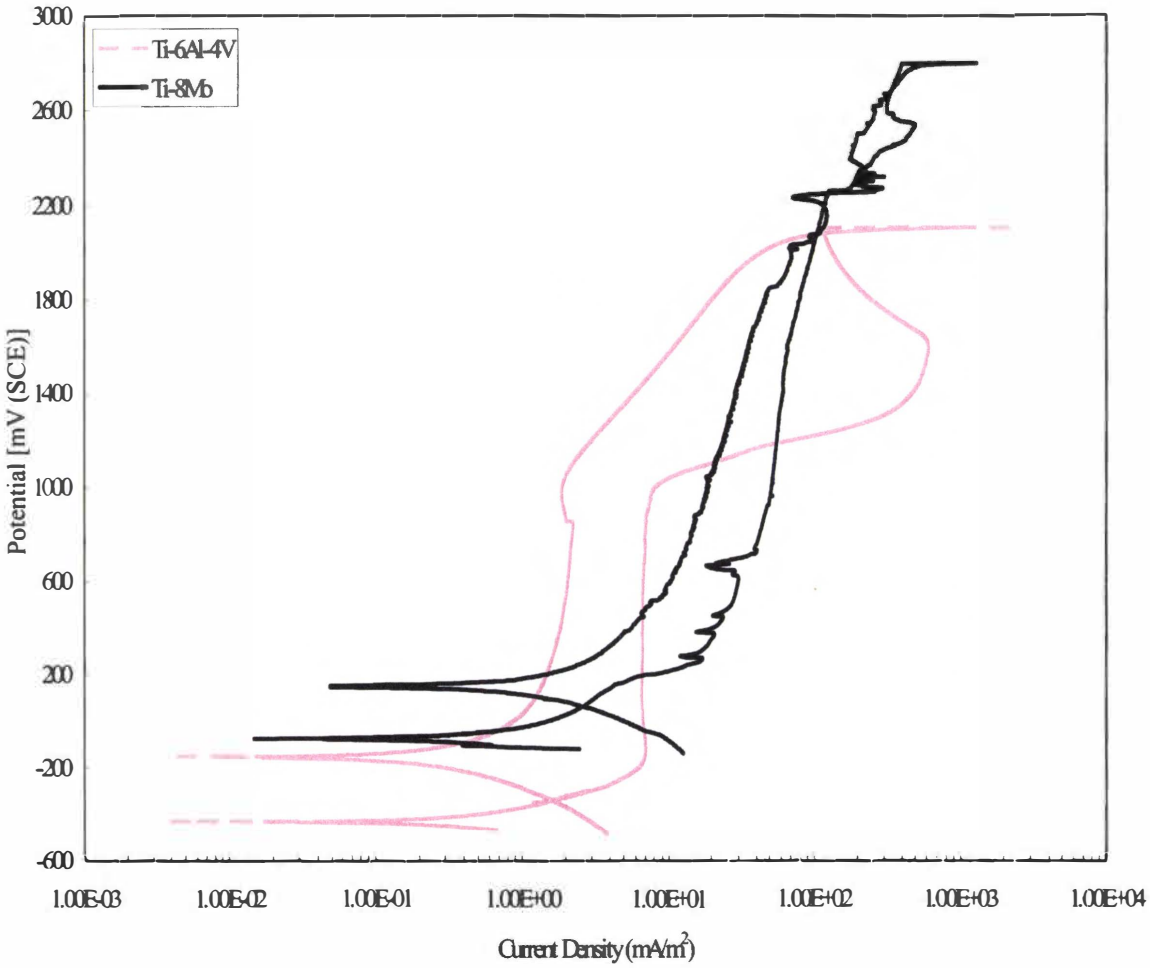

Figure 21. Cyclic-anodic-polarization curves of Ti-6Al-4V and Ti-8Mo. This figure shows representative curves for both alloys.

APPENDIX OF MATLAB CODE

%% Matlab Code Used to Analyze The Worn Surface of Metals

%% Authors: Chris Stephens & Brandice Green

%% VARIABLES %%

%% ~ d = worksheet in Excel that is being referenced (This file path is inputed in the command window)

%% ~ sheet_unmod = This is the sheet in Excel that your unmodified data, minus the wear track is stored.

%% ~ sheet_wear = This is the sheet in Excel where your wear data is stored

%% ~ a_unmod = This is the two column matrix generated by MATLAB with the data exported from sheet_unmod (If there are titles above your data columns, they will be ignored. *DO NOT LEAVE CELLS THAT ARE BLANK AT THE TOP OF THE WORKSHEET).

%% ~ a_wear = This is the two column matrix generated by MATLAB with the data exported from sheet_wear (If there are titles above your data columns they will be ignored).

%% ~ x_unmod = This takes the first column for the a_unmod matrix and makes a new one column matrix called x_unmod.

%% ~ y_unmod = This takes the second column for the a_unmod matrix and makes a new one column matrix called x_unmod.

%% ~ x_wear = This takes the first column for the a_wear and makes a new one column matrix called x_wear.

%% ~ y_wear = This takes the second column for the a_wear matrix and makes a new one column matrix called x_wear.

%% ~ n = The degree of the polynomial used to fit the unmodified data.

%% ~ p = This generates the coefficients needed for the polynomial fit.

%% ~ y_fit = This is the polynomial generated by n and p evaluated at x_wear.

%% ~ y_difference = This is the height change between the best fit line on the unmodified data and the wear track. (y-fit is evaluated at the x_wear so y_difference can be obtained.

%% ~ f = area between the linear fit on the unmodified (evaluated at the wear x-values) and the wear y-values

%% ENTERED DATA %%

% Clears all previous setting

```
clc;
clear all;
```

%% LOADS DATA FROM EXCEL %%

```
d=input('Specify the file you would like to analyze: \n','s');
sheet_unmod=input('\nSpecify the sheet in Excel that you would like \nto use to analyze the unmodified surface: \n','s');
sheet_wear=input('\nSpecify the sheet name that you would like \nto use to analyze the wear surface: \n','s');
a_unmod=xlsread(d,sheet_unmod);
a_wear=xlsread(d,sheet_wear);
```

% Seperation of the Matrix

```
x_unmod=a_unmod(:,1);
y_unmod=a_unmod(:,2);
x_wear=a_wear(:,1);
y_wear=a_wear(:,2);
```

%% CALCUALTIONS %%

% Calculate the best fit curve for unmodified data

```
n = 3;
p = polyfit (x_unmod,y_unmod,n);
y_fit = polyval(p,x_wear);
```

% Calculate the height change between the linear fit of the unmodified data and the wear track

```
y_difference = y_fit-y_wear;
```

% Calculate the numerical integral using y_difference and x_wear.

```
f=0;
for i=1:length(x_wear)-1
```

```
   f=f+y_difference(i).*(x_wear(i+1)-x_wear(i));
end
```

%% GRAPHICS %%

```
figure(1)
plot(x_unmod,y_unmod,'g', x_wear,y_wear,'b', x_wear,y_fit,'k-')
axis([-50 x_unmod(len h(x_unmod))+50 min(y_wear)+.2*min(y_wear)
max(y_unmod)+.1*max(gty_unmod)]);
title('Profilometry Analysis of Metals')
xlabel('Sliding Distance (Microns)')
ylabel('Height (Microns)')
legend('Unmodified Data', 'Wear Data', 'Best-Fit Line on Unmodified Data')
text(0,min(y_wear)+.05*min(y_wear),['BEST-FIT LINE: (',num2str(p(1),6),')x +
(',num2str(p(2),6),')'])
text(0,min(y_wear)+.1*min(y_wear),['AREA OF METAL REMOVED DURING WEAR
                    TEST: ',num2str(f(1),6),' Square Microns'])
```

VITA

Brandice Annette Green was born in Georgetown, South Carolina in 1980. She was raised in Memphis, TN and attended grade school at Harding Academy. She attended White Station Middle School and White Station High School. In 1998, she graduated from White Station High School and went on to attend The University of Tennessee, Knoxville. She received a B.S. in Materials Science and Engineering in 2002 and a M.S. in Materials Science and Engineering in 2004.